CZECH TECHNICAL UNIVERSITY IN PRAGUE

Faculty of Electrical Engineering

Diploma thesis

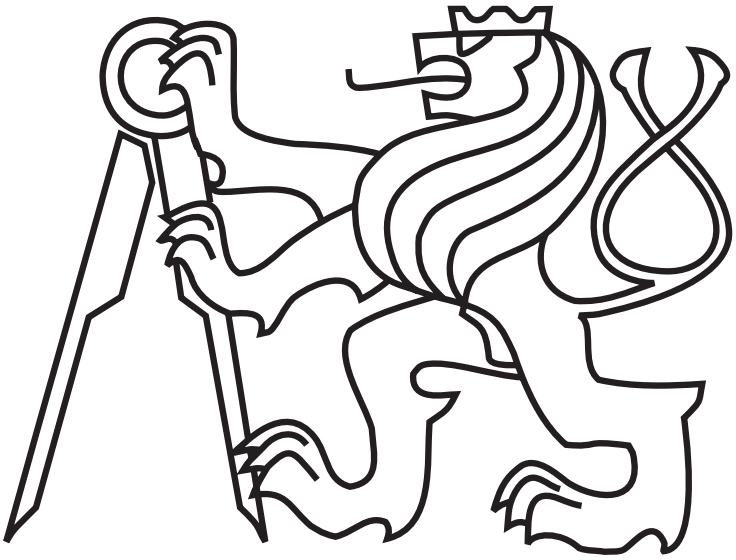

Bc. Adam Třešňák

Forces Acting on the Robot during Grinding

Department of Cybernetics

Thesis supervisor: **Ing. Vladimír Smutný, Ph.D.**

Prague, May 2017

Czech Technical University in Prague
Faculty of Electrical Engineering

Department of Cybernetics

DIPLOMA THESIS ASSIGNMENT

Student: Bc. Adam T ř e š ň á k

Study programme: Cybernetics and Robotics

Specialisation: Robotics

Title of Diploma Thesis: Forces Acting on the Robot during Grinding

Guidelines:

1. Search for the literature describing forces acting during machining and use of industrial manipulators for machining.
2. Model the forces and moments acting on the robot both from static and dynamic forces during machining.
3. Perform simulation for chosen trajectories and applied forces.
4. Build simple grinding tool, mount it to the robot and measure forces and moments.
5. Compare the results of simulation and experiment and make conclussions.

Bibliography/Sources:

[1] Mark W. Spong and M. Vidyasagar: Robot Dynamics and Control. John Wiley & Sons, 1989.
[2] Reza Jazar: Theory of Applied Robotics: Kinematics, Dynamics, and Control. Springer, 2007.
[3] Yonghua Chen, Fenghua Dong: Robot machining: recent development and future research issues, The International Journal of Advanced Manufacturing Technology, June 2013, Volume 66, Issue 9, pp 1489-1497.

Diploma Thesis Supervisor: Ing. Vladimír Smutný, Ph.D.

Valid until: the end of the summer semester of academic year 2017/2018

L.S.

prof. Dr. Ing. Jan Kybic
Head of Department

prof. Ing. Pavel Ripka, CSc.
Dean

Prague, October 24, 2016

Abstract

This thesis deals with the forces acting on an industrial robot manipulator during metal machining with a machining tool mounted at the position of an end-effector. The machining is performed by grinding of a material with a rotating abrasive disc. Both static and dynamic forces acting on the robot during machining are modelled using the Recursive Newton-Euler Algorithm for dynamic modelling of rigid-bodies. The simulations for chosen trajectories of the machining tool are performed in order to investigate the influence of a gyroscopic effect (among other things). This effect arises during the manipulation with heavy rotating masses of the machining tool and it can have a negative influence on the structure of manipulator or even cause its damage. Based on the results of simulations, the capability of the industrial manipulator KUKA KR 500 R2830 MT (namely its actuators) to perform the machining operation is discussed. The implemented solution to the dynamic modelling of robot manipulators as well as the suitability of used method is verified in an experiment with real robot with similar structure.

keywords: [industrial manipulator, dynamics, Newton-Euler algorithm, KUKA KR 500, grinding, machining, gyroscopic effect]

Abstrakt

Tato práce se zabývá silami působícími na průmyslový manipulátor při obrábění kovového materiálu nástrojem připevněným na poslední ose robotu. Obrábění je realizováno broušením materiálu brusným kotoučem. Dynamické chování manipulátoru během broušení je modelováno pomocí rekurzivního Newton-Eulerova algoritmu. Pro vybrané trajektorie brusného nástroje jsou provedeny simulace, prostřednictvím kterých je mimo jiné zkoumán vliv gyroskopického momentu na pohony robotu. Gyroskopický moment při broušení vzniká jako důsledek manipulace s rychle se otáčejícím brusným kotoučem upevněným spolu s dalšími rotujícími hmotami na posledním rameni manipulátoru. Důsledkem tohoto působení pak může docházet k nadměrnému mechanickému namáhání dílů a některých pohonů robotu, případně i k jejich poškození. Na základě výsledků simulací a známých limitů pohonů manipulátoru je diskutováno namáhání pohonů průmyslového robotu KUKA KR 500 R2830 MT během broušení a obecně vhodnost tohoto manipulátoru pro tento typ úlohy. Implementované řešení a vhodnost použité metody modelující dynamické chování robotu při broušení jsou ověřeny pomocí experimentu s reálným robotem podobné konstrukce.

klíčová slova: [průmyslový manipulátor, dynamika, Newton-Eulerův algoritmus, KUKA KR 500, broušení, obrábění, gyroskopický jev]

Declaration

I declare that the presented work was developed independently and that I have listed all sources of information used within it in accordance with the methodical instructions for observing the ethical principles in the preparation of university theses.

Prague, date ....

Acknowledgements

I would like to thank my supervisor Ing. Vladimír Smutný, Ph.D. for his assistance throughout the writing of this thesis. I especially appreciate his helpful advices, provided materials, many useful insights and relevant discussion during our regular meetings.

I am very grateful to my friends, close relatives and especially to my parents for supporting me during my entire study.

Contents

List of Figures

1 Introduction

Robotics is an interdisciplinary branch of engineering and science that involves the design, construction, and operation of robots. This field includes mechanical engineering, electrical engineering, electronics, computer science, artificial intelligence, mechatronics, and many others.

One of the definitions of the term *robot* comes from the year 1979. The Robot Institute of America defined the robot as *a reprogrammable, multifunctional manipulator designed to move material, parts, tools, or specialized devices through various programmed functions for the performance of a variety of tasks.* This definition is especially accurate for the field of industrial robotics.

The history of industrial robotics dates back to the year 1954, when George Charles Devol invented the first industrial robot - the Unimate. It was a robotic arm used to extract hot parts from a die-casting machine, which was a dangerous job for a human worker. The robot manipulators eventually replaced humans for the heavy, dangerous and monotonous tasks and they are nowadays widely used in factories to perform high-precision jobs such as welding, riveting or assembly.

1.1 Motivation

The industrial manipulators are also deployed in metallurgy. In this branch of industry, robots are typically used either for a manipulation with the workpieces or for their manufacturing such as deburring or grinding. The latter named procedure, namely the grinding of an edge of a steel billet using a grinding disc, is the main subject of interest in this thesis.

In general, there are two methods how to perform grinding with an industrial manipulator. The first option is to grasp the workpiece with a gripper mounted on the robot and to perform the process of grinding on a stationary grinding device by pushing the workpiece against an abrasive. However, this method is suitable mainly for smaller light-weight workpieces. The second option is to mount the grinding device on the manipulator and to perform the grinding by pushing the tool against the workpiece, which is the case considered in further text.

The thesis is concerned with the influence of the rotating masses (grinding disc, grinding tool shaft etc.), which are located at the position of an end-effector, on the actuators of the manipulator. This fast rotation in combination with other movements of the manipulator is expected to generate a gyroscopic effect, which is assumed to have an influence on the entire structure of the manipulator.

The ultimate goal should be the analysis if the actuators of suggested industrial manipulator KUKA KR 500 R2830 MT are capable to perform the grinding operation. A choice and an application of appropriate method for modelling of dynamics of serial manipulators and its verification in an experiment can be named as the inferior goals of this thesis.

It seems to be fair to note, that dynamic modelling of an industrial manipulator is quite demanding and complex task, which cannot be solved by hand with use of simple mathematical expression. Even more challenging than the modelling of dynamics itself is the optimization of the position of the manipulator with respect to the position of the workpiece, to size and reach of the manipulator or to its position with respect to other components of a production line.

1.2 Thesis Layout

- **Chapter 2** describes the grinding task for the robot manipulator as well as the current solution of grinding of the steel billets. An overview of the literature search for similar applications is presented.
- **Chapter 3** introduces the suggested industrial manipulator produced by KUKA AG and provides an insight into its kinematic description. Furthermore, the process of an estimate of the parameters necessary for the simulation of dynamics is described.
- **Chapter 4** deals with the method of dynamic modelling of robot manipulators. There are briefly discussed different approaches and an insight into the Newton-Euler formulation is provided in detail. Brief description of the gyroscopic effect and an example, which demonstrates its influence, are also presented in this chapter.
- **Chapter 5** is concerned with the dynamic simulations of suggested manipulator modelled using the Newton-Euler approach. A short introduction into the metal grinding for the purpose of simulation is presented and a result of the simulation is discussed in detail.
- **Chapter 6** describes an experiment with a real robot and a simple model of the grinding tool. The main goal of the experimental measurement is to verify the validity of implemented solution.
- **Chapter 7** contains a conclusion of reached results and some recommendations related to the future work.

2 | Task Description

A processing of a material in the a rolling mill and its relation to the grinding of the steel billet with the industrial manipulator is introduced in this chapter. In the second section, an overview of the literature dealing with similar application is presented.

2.1 Problem Definition

In the hot rolling mills, long products (e.g. wire rods, bars, rails or billets) are fabricated by rolling. The hot rolling mill shown in Figure 2.1 consists of a reheating furnace, a descaling unit, a roller conveyor, a hot mill stand and a cooling bed.

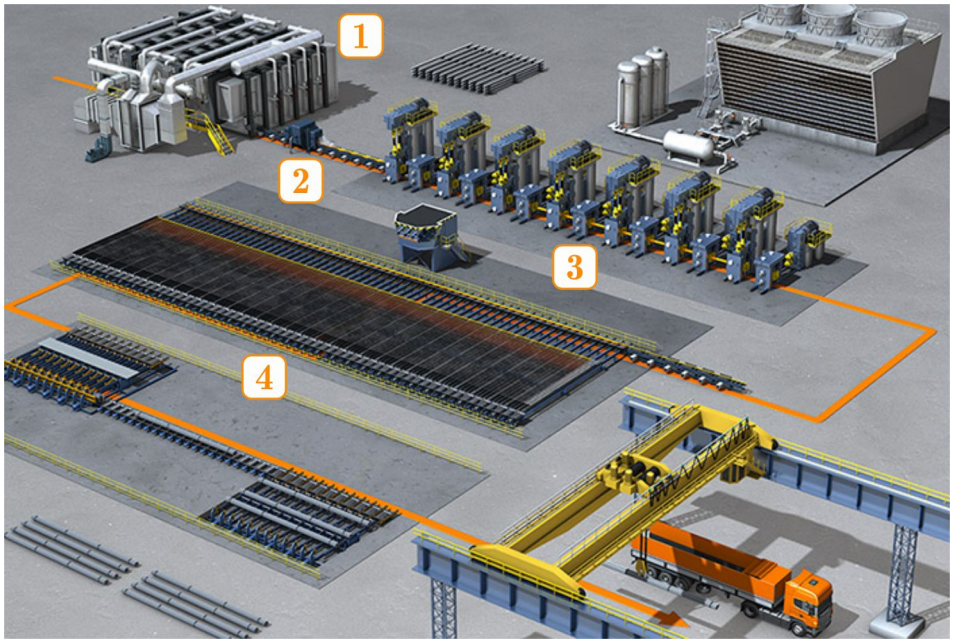

Figure 2.1: Hot rolling mill [1]

At first, the input metal ingots are heated to a temperature above the recrystallization temperature in the reheating furnace (number 1 in Figure 2.1). As the required temperature of the ingot is reached, it is taken out of the furnace and the descalers (number 2) blast the metal surface with pressurized water. This procedure removes the oxide scale, which occurs when the heated steel is exposed to the oxygen in the air. Further, the heated steel is formed into a required shape by continuous compression between two rolls rotating in the opposite direction at the hot mill stand (3). Once the billets have been formed, they can be cut into the parts of

different length according to the customer's specification. A cutting device is not drawn in the picture, but it is situated between the hot mill stand and the cooling beds. On the cooling beds (4), the billets cool down homogeneously on their way from the hot rolling mill to the finishing line. The function of the rolling mill, that was described above, is completely based on [1].

The cutting of the metal produces the burrs of different size and shape at the edge of the section through the material (see Figure 2.2). These burrs have to be removed in order to provide a high quality production. Besides a bad look, there is also a risk of an injury during the manipulation with such material.

(a) Billets with circular cross-section

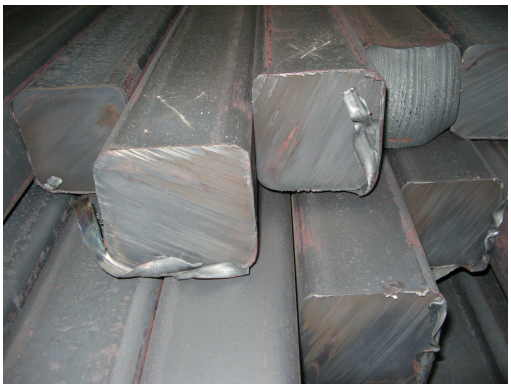

(b) Billets with quadratic cross-section

Figure 2.2: Burrs at the edge of section through the billet [2]

A machining of the burrs is currently performed by a grinding machine shown in Figure 2.3. The billet is delivered by a conveyor to the grinding station. Then, it is aligned to an end-stop shown in the right part of the picture. As the next step, the conveyor shifts the billet under the grinding disc and the grinding operation is executed. The rotating grinding disc is lowered down at the edge of the billet and the billet is then rotated around its axis about 360 degrees. The billets after the manufacturing of the edge are shown in Figure 2.4.

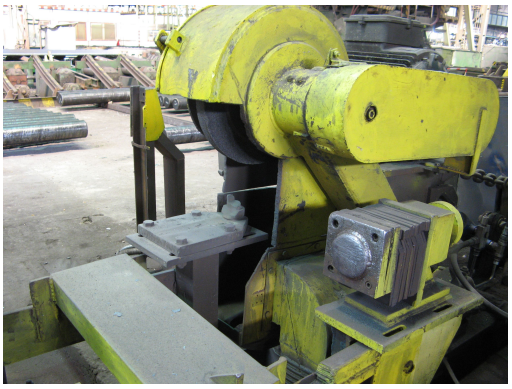

Figure 2.3: Current grinding station [2]

Apparently, only the billets with the circular cross-section can be ground this way. Those with the quadratic section have to be manufactured by hand. This is the main drawback of the current grinding technology. Moreover, there is no guarantee that the grinding machine executes uniform grinding around the entire circumference (see the highlighted area in Figure 2.4a) since it is pushed against the billet with a constant force.

(a) Ground billet

(b) Billet gound by hand

Figure 2.4: Ground billets [2]

Current grinding station is supposed to be replaced with a six-axis industrial robot manipulator with a grinding tool mounted on its flange as the end-effector. This would allow the billets with both circular and quadratic cross-sections to be ground. Such a solution provides a great variability of an application as the next benefit. There would be almost no limits to different sizes and shapes of the billets. A variability of the grinding angle can be named as the next advantage. On the other hand, industrial manipulator capable of holding a similar grinding device requires much more operational space than presented simple grinding station. A manipulation with a heavy rotating mass represented by the grinding disc appears to be more complicated than relatively simple rotation with the billet. The influence of gyroscopic effect has to be taken into account during the task of grinding with the manipulator. Fast changes of orientation of the grinding tool produce a torque generated by gyroscopic precession. The magnitude of this torque could damage or even destroy the manipulator and possibly cause a serious injury in case of an excessive fast manipulation. The influence of these forces and torques on the actuators of the manipulator are simulated and discussed in the latter chapters.

2.2 State of the Art

The use of the robots as the machining systems contains many subtasks such as machining path planning, dynamics modelling, vibration and chatter analysis, stiffness modelling, and many others. There have been already presented some publications and articles dealing with the machining using a six-axis robot manipulators. The authors in [5] describe the rapid prototyping based on machining, vibration and chatter analysis and path planning for the machining operation. The dynamic model of the manipulator ABB IRB 6400 obtained by a system identification and its control as well as the robot stiffness modelling are presented in [6]. The chatter analysis of robotic machining process [7] investigates the onset of chatter problem and principles to prevent that issue. Another work [8] deals with the force control of the robot ABB IRB 4400/45 during polishing and deburring.

All previously named publication have in common the use of relatively small and light-weight tolls for the processes of polishing, deburring or machining. Used machining tools, spindles, drills or milling machines have negligible moments of inertia and masses in comparison with suggested grinding disc for the application described in previous section. Moreover, there was possible a direct measurement on the real robot manipulator in order to identify its accurate dynamic model in some previously named publications.

3 System Description

The serial industrial six-axis robot manipulator KUKA KR 500 R2830 MT has been suggested for the purpose of the task described in Section 2.1. At first, the proposed manipulator is introduced in this chapter. Further, its kinematics is described and a solution of direct and inverse kinematic task is briefly discussed. As the manipulator is supposed to be used in dynamic simulations, its kinematics is not the sufficient description. The dynamic parameters, which are necessary for dynamic simulations, have to be determined for each link. Since this information is not known, a method for the estimate of these parameters is presented.

3.1 Manufacturer Information

The KUKA KR 500 series robot manipulator shown in Figure 3.1 is an open-chain kinematic structure with six degrees of freedom created by a base and six links joined together by six revolute joints. Last three joints create a 3-axis in-line wrist (axes of last three joints have a common intersection). Such a construction allows the manipulator to reach any position and orientation of an end-effector in its workspace. Each of the six joints (axis) of the manipulator is driven by an AC servo motor. Components of the body of the robot are made of light alloy and iron castings. There is also a hydropneumatic counterbalancing system mounted between the rotating column (link 1) and the link arm (link 2). This device is used to minimize the torques generated about second axis when the robot is moving or stationary. Such a device has a significant impact in case of industrial manipulators, which are supposed to manipulate with heavy payloads. KUKA KR 500 is able to operate with the payload up to 500 kilograms.

Figure 3.1: KUKA KR 500 R2830 MT [3]

3.2 Description of Kinematics

The description of kinematics of the robot manipulator is based on a documentation provided by the manufacturer. A technical drawing with the dimensions of the robot and describing a workspace of the robot is shown in Figure 3.2.

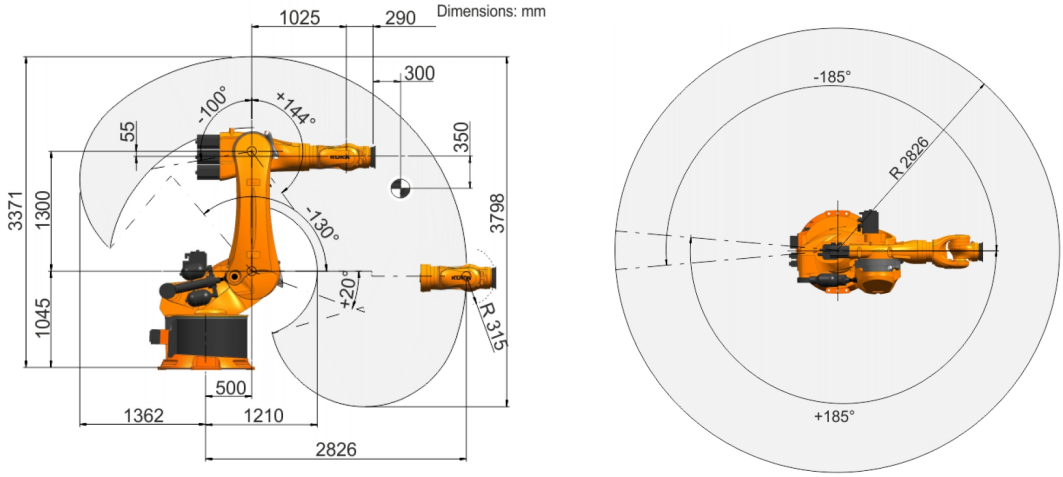

(a) Left view (b) Top view

Figure 3.2: KUKA KR 500 dimensions (drawing) [4]

The robot manipulator has been described using the Denavit-Hartenberg notation [9]. It is an effective convention for attaching reference frames to the links of a robot. Parameters of this notation that have been found are written in Table 3.1. Note, that symbols q_i represent the joint coordinates (positions) measured by the sensors in the joints of the manipulator. Attached reference frames (their z-axis respectively, according to the convention) should respect the directions of rotation of the actuators (see Figure 3.3). Frames attached to the manipulator according to this convention are shown in Figure 3.4. The D-H notation is particularly useful while solving both direct and inverse kinematic tasks for the manipulator.

i	θ_i[rad]	d_i[m]	a_i[m]	α_i[rad]	$\theta_{\text{offset},i}$[rad]
1	q_1	-1.045	0.500	$\frac{\pi}{2}$	0
2	q_2	0	1.300	0	0
3	q_3	0	0.055	$-\frac{\pi}{2}$	$\frac{\pi}{2}$
4	q_4	-1.025	0	$\frac{\pi}{2}$	0
5	q_5	0	0	$-\frac{\pi}{2}$	0
6	q_6	-0.290	0	π	0

Table 3.1: Denavit-Hartenberg parameters

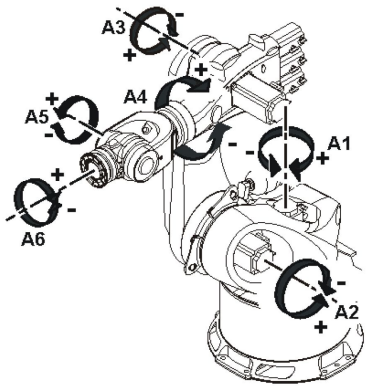

Figure 3.3: Axes orientation [4]

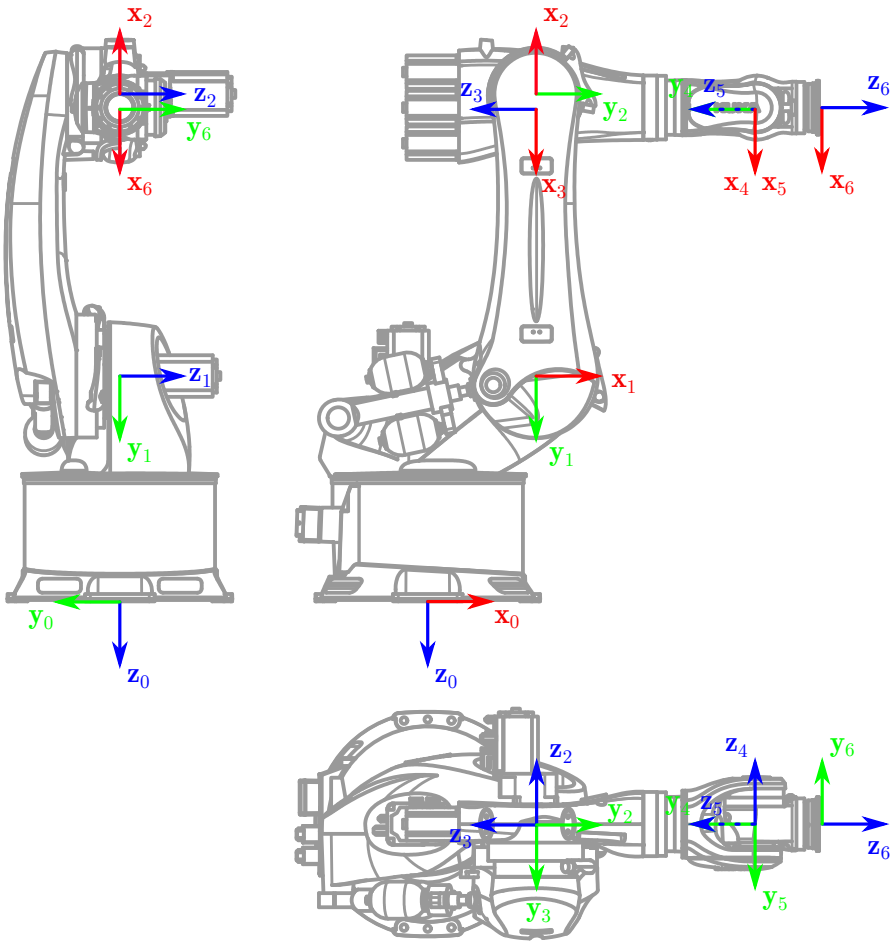

Figure 3.4: Attached reference frames according to the D-H notation

Direct Kinematic Task

The direct (forward) kinematic task is a mapping from a joint coordinate space to a space of positions of the end-effector using the kinematic equations of the particular manipulator [10]. The problem of direct kinematics can be expressed as a function

$$\boldsymbol{r} = f(\boldsymbol{q}) \tag{3.1}$$

where $\boldsymbol{r}$ represents coordinates of (usually) the Cartesian space, $\boldsymbol{q}$ describes joint coordinates (positions) measured by the robot and f stands for the mapping function.

A systematic method solving the direct kinematic task assigns the reference frames to the robot links and uses homogeneous transformation matrices to express the relations between them. The result of this task is a position of the end-effector in space based on knowledge of actual joint coordinates.

Transformation $\boldsymbol{A}$ between two consecutive reference frames $i-1$ and i described by Denavit-Hartenberg notation can be described using four parameters from Table 3.1. Such a transformation can be calculated as

$$\boldsymbol{A}_i^{i-1} = \boldsymbol{A}_{i'}^{i-1}\boldsymbol{A}_i^{i'} \tag{3.2}$$

Matrix $\boldsymbol{A}_{i'}^{i-1}$ describes rotation and translation around and along the axis z_{i-1} while matrix $\boldsymbol{A}_{i}^{i'}$ (which is always a constant matrix) represents rotation and translation around and along the axis x_i. The transformation between successive frames (Equation 3.4) is then created by multiplication of these two matrices.

$$\boldsymbol{A}_{i'}^{i-1} = \begin{bmatrix} \cos\theta_i & -\sin\theta_i & 0 & 0 \\ \sin\theta_i & \cos\theta_i & 0 & 0 \\ 0 & 0 & 1 & d_i \\ 0 & 0 & 0 & 1 \end{bmatrix} \qquad \boldsymbol{A}_{i}^{i'} = \begin{bmatrix} 1 & 0 & 0 & a_i \\ 0 & \cos\alpha_i & -\sin\alpha_i & 0 \\ 0 & \sin\alpha_i & \cos\alpha_i & 0 \\ 0 & 0 & 0 & 1 \end{bmatrix} \tag{3.3}$$

$$\boldsymbol{A}_{i}^{i-1} = \begin{bmatrix} \cos\theta_i & -\sin\theta_i\cos\alpha_i & \sin\theta_i\sin\alpha_i & a_i\cos\theta_i \\ \sin\theta_i & \cos\theta_i\cos\alpha_i & -\cos\theta_i\sin\alpha_i & a_i\sin\theta_i \\ 0 & \sin\alpha_i & \cos\alpha_i & d_i \\ 0 & 0 & 0 & 1 \end{bmatrix} \tag{3.4}$$

The entire solution of the direct kinematics is then performed as the multiplication of transformation matrices $\boldsymbol{A}_{i}^{i-1}$ for all pairs of consecutive reference frames in the system according to following equation

$$\boldsymbol{x}_0 = A_1^0(q_1)A_2^1(q_2)A_3^2(q_3)\ldots A_n^{n-1}(q_n)\boldsymbol{x}_n \tag{3.5}$$

where $\boldsymbol{x}_0$ denotes base-frame coordinates of point $\boldsymbol{x}_n$, which has been expressed in n-th (end-effector) reference frame, and q_i represents variable parameter θ_i (in case of revolute joints).

Inverse Kinematic Task

The inverse kinematic task is a mapping from the space of positions (and orientations) of the end-effector to the space of joint coordinates. The meaning of symbols in following expression describing the inverse kinematics is the same as in previous case of the direct kinematic task.

$$\boldsymbol{q} = f^{-1}(\boldsymbol{r}) \tag{3.6}$$

In other words, the joint coordinates for a given position and orientation of the end-effector should be found. In general, there are two methods for solving the inverse kinematics: analytical and numerical. The analytical solution is always preferred, if it can be found. Moreover, it provides more than one solution for given end-effector pose (position and orientation). A sufficient condition for using the analytical solution for the six-axis manipulator is the case when the robot has three consecutive revolute joints with axes intersecting in one point [11]. This condition is fulfilled for the manipulator KUKA KR 500, so the inverse kinematic task for this particular manipulator can be solved this way. However, the solution of inverse kinematics is just an inferior subtask of this thesis and it basically follows the steps described in [11], thus it will not be elaborated any further in this text.

3.3 Grinding Tool

There is supposed to be a grinding tool mounted on the manipulator. As the final one is not known yet a simple model of grinding tool drawn in Figure 3.5 has been designed for the

purposes of this thesis. It consists of three-phase asynchronous motor (green part), a coupling (blue part) and a grinding disc (grey part) and it is basically a copy of the current grinding station shown in Figure 2.3. The entire device is mounted on the flange (the sixth i.e. the last link) of the robot (see Figure 5.1). For further purposes, this device (its grinding disc, respectively) is considered to be an end-effector. In this case, the shaft of the grinding tool represents the seventh axis (joint) of the manipulator, while the grinding disc represents the seventh link. This approach allows the intuitive deployment of the Newton-Euler algorithm. The Denavit-Hartenberg notation has to be modified and extended in order to attach the reference frames to each new link of the robot system (see Table 3.2). The frames of last two links of the system are drawn in Figure 3.5b. Suggested device containing the three components described above has a weight of approximately 250 kilograms.

$\boldsymbol{i}$	θ_i[rad]	d_i[m]	a_i[m]	α_i[rad]	$\theta_{\text{offset},i}$[rad]
6	q_6	-0.520	0	$-\frac{\pi}{2}$	0
7	q_7	0.445	0	0	0

Table 3.2: Denavit-Hartenberg parameters considering the grinding tool

There is a red point at the circumference of the disc pictured in Figure 3.5b, which represents a contact point of the disc with the ground material. This point has a fixed position in the coordinate frame of the tool, not in the frame of the rotating disc (i.e. the position of the reference point does not change when the disc starts its rotational movement). Although the designed grinding tool in the simulation can be arbitrary oriented around its z-axis to achieve the same machining effect, in the real industrial application there is supposed to be a protective cover around the disc. This cover does not allow to change the orientation of the grinding tool, since only a small part of the disc remains uncovered and this part has a fixed position with respect to coordinate frame of the tool. The highlighted reference point has been chosen for the simulations presented in this thesis.

The machining procedure uses the longitudinal edge grinding technique with a spindle axis parallel to the ground edge in case of rectangular billet. In case of the circular one, the axis is analogically oriented in the tangential direction.

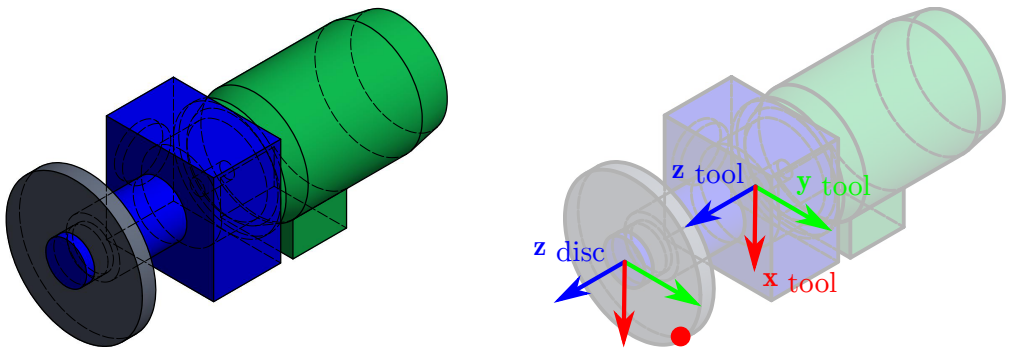

(a) 3D model [2]

(b) Coordinate frames and the contact point

Figure 3.5: Grinding tool model

3.4 Dynamic Parameters Estimation

Besides common parameters (dimensions required for DH-notation and in some cases maximum allowable torque in every actuator), the dynamic simulations require some further information such as moments of inertia, a center of gravity, and a mass of each link of manipulator, which are not usually included in the manufacturer specification of a respective robot. Those parameters have an essential influence on the results of simulations. Since the manufacturer typically does not provide these additional specifications even on a request, the dynamic parameters have to be estimated as accurately as possible.

Different Approaches

The most precise way how to estimate the dynamic parameters of a robot manipulator (besides the information provided by manufacturer), would be performing a dynamic parameter identification of a real manipulator as presented in [12] or [13]. Unfortunately, referenced materials deal with other types of manipulators, namely with KUKA LBR iiwa and KUKA youBot. Moreover, the dynamic parameter identification is quite demanding task and it requires a direct access to the real manipulator.

Another (less accurate) method is to substitute every link of robot manipulator with a simple volume, whose dynamic parameters are known or easy to compute. The most convenient volume for this case could be a cylinder with uniformly distributed mass. There are two significant uncertainties besides the fact, that the shape of cylinder is really rough approximation of the shape of links of the manipulator. First, the mass of each cylinder would have to be estimated based on the total weight of the manipulator, which is the information provided by the manufacturer. Second, the links of the real manipulator certainly have not uniformly distributed mass in the entire volume of the respective link. Hollow cylinder could fix this issue but the thickness of such cylinder would be still a rough guess.

The use of a 3D CAD model of respective robot manipulator and a suitable software (for example CATIA or Autodesk Inventor) appears to be the most precise available attitude to estimate required dynamic parameters without actual access to the real manipulator. The models are typically provided by the manufacturers and are usually available on their websites. Depending on the details of provided 3D models, one is able to estimate required parameters.

Parameters Estimate using Autodesk Inventor

Required unknown parameters of the robot have been estimated based on the 3D CAD manipulator model in the *STL* format. The major drawback of provided model is its format. As the *STL* (STereoLithography) file describes only the surface geometry of a three-dimensional object, there is missing information about the thickness of chassis of particular links, used materials and inner components of the manipulator. Still, detailed description of shapes of links grants more accurate estimate than the approximation of links by solid cylinders.

Autodesk Inventor is able to compute a volume of constructed body even if the body is specified by its surface. The entire model of the manipulator has been separated into individual links and the volume of each link has been determined. A weight of each link has been estimated based on the ratio of volumes of all links and known weight of entire robot manipulator, which is approximately 2440 kg according to the manufacturer's information. Autodesk Inventor computes the position of the center of gravity and the inertia matrix using the shape of the volume and its mass, which is considered to be uniformly distributed across the entire volume.

Parameters that have been found for the dynamic simulations are listed in the following overview. The matrices of tensors of inertia as well as the position vectors of the center of gravity for individual links are described with respect to the coordinate frames of the individual links (see Figure 3.4).

$$m_{\text{base}} \approx 945 \text{ [kg]}$$

$$\boldsymbol{r}_{\text{base,COG}} = [-0.018, 0, -0.289]^T \text{ [m]}$$

$$\boldsymbol{I}_{\text{base}} = \begin{bmatrix} 71.366 & -0.116 & -0.671 \\ -0.116 & 79.321 & -0.014 \\ -0.671 & -0.014 & 101.746 \end{bmatrix} \text{ [kg} \cdot \text{m}^2\text{]}$$

$$m_1 \approx 558 \text{ [kg]}$$

$$\boldsymbol{r}_{1,\text{COG}} = [-0.409, 0.205, 0.035]^T \text{ [m]}$$

$$\boldsymbol{I}_1 = \begin{bmatrix} 31.479 & -11.062 & 9.269 \\ -11.062 & 59.845 & 1.849 \\ 9.269 & 1.849 & 65.161 \end{bmatrix} \text{ [kg} \cdot \text{m}^2\text{]}$$

$$m_2 \approx 485 \text{ [kg]}$$

$$\boldsymbol{r}_{2,\text{COG}} = [-0.847, 0, -0.310]^T \text{ [m]}$$

$$\boldsymbol{I}_2 = \begin{bmatrix} 13.322 & 11.567 & -0.293 \\ 11.567 & 113.722 & -0.251 \\ -0.293 & -0.251 & 112.739 \end{bmatrix} \text{ [kg} \cdot \text{m}^2\text{]}$$

$$m_3 \approx 311 \text{ [kg]}$$

$$\boldsymbol{r}_{3,\text{COG}} = [-0.033, -0.010, 0.043]^T \text{ [m]}$$

$$\boldsymbol{I}_3 = \begin{bmatrix} 27.449 & -0.109 & -0.301 \\ -0.109 & 25.058 & 0.980 \\ -0.301 & 0.980 & 10.561 \end{bmatrix} \text{ [kg} \cdot \text{m}^2\text{]}$$

$$m_4 \approx 86 \text{ [kg]}$$

$$\boldsymbol{r}_{4,\text{COG}} = [0, 0.266, -0.011]^T \text{ [m]}$$

$$\boldsymbol{I}_4 = \begin{bmatrix} 2.783 & 0 & 0.172 \\ 0 & 3.471 & 0 \\ 0.172 & 0 & 1.423 \end{bmatrix} \text{ [kg} \cdot \text{m}^2\text{]}$$

$$m_5 \approx 48 \text{ [kg]}$$

$$\boldsymbol{r}_{5,\text{COG}} = [0, -0.038, -0.052]^T \text{ [m]}$$

$$\boldsymbol{I}_5 = \begin{bmatrix} 0.700 & 0 & 0 \\ 0 & 0.684 & 0.112 \\ 0 & 0.112 & 0.438 \end{bmatrix} \text{ [kg} \cdot \text{m}^2\text{]}$$

$$m_6 \approx 7 \text{ [kg]}$$

$$\boldsymbol{r}_{6,\text{COG}} = [0, 0, -0.027]^T \text{ [m]}$$

$$\boldsymbol{I}_6 = \begin{bmatrix} 0.018 & 0 & 0 \\ 0 & 0.018 & 0 \\ 0 & 0 & 0.034 \end{bmatrix} \text{ [kg} \cdot \text{m}^2\text{]}$$

The estimated parameters for the sixth link have to be modified in case there is the grinding tool considered to be mounted on the flange. In the same case, parameters for the seventh link (grinding disc, rotor shaft and rotor winding) have to be added.

$$m_{6(\text{tool})} \approx 260 \text{ [kg]}$$

$$\boldsymbol{r}_{6(\text{tool}),\text{COG}} = [0.008; -0.007; -0.195]^T \text{ [m]}$$

$$\boldsymbol{I}_{6(\text{tool})} = \begin{bmatrix} 26.763 & 0.013 & 0.223 \\ 0.013 & 26.770 & -0.329 \\ 0.233 & -0.329 & 6.286 \end{bmatrix} \text{ [kg} \cdot \text{m}^2\text{]}$$

$$m_7 \approx 75 \text{ [kg]}$$

$$\boldsymbol{r}_{7,\text{COG}} = [0, 0, -0.3015]^T \text{ [m]}$$

$$\boldsymbol{I}_7 = \begin{bmatrix} 1.448 & 0 & 0 \\ 0 & 1.448 & 0 \\ 0 & 0 & 1.220 \end{bmatrix} \text{ [kg} \cdot \text{m}^2\text{]}$$

4 Dynamic Modelling of Robot Manipulators

Robot dynamics describes the relationship between the forces acting on a robot mechanism and the motion, which is produced by these forces. Typically, the robot mechanism is considered as a rigid-body system, which allows to use the rigid-body dynamic approach directly to the respective robot manipulator. The content of this chapter presents general facts about dynamic modelling and introduces the core of the Recursive Newton-Euler Algorithm, which is a suitable tool for this task. Further, the gyroscopic effect, which appears during the manipulation with quickly rotating body, is described. At the end, a dynamic model of a flywheel is built using presented algorithm.

4.1 Dynamic Modelling in General

Basically, the dynamics related to the robot manipulators can be divided into two main problems. **Forward dynamics** deals with the problem of finding the acceleration response of given (rigid-body) system influenced by forces and torques acting on the system. This procedure is used mainly in computer simulations. On the other hand, with the use of **inverse dynamics** one is able to find forces and torques required to produce given motion specified by acceleration response of each body in the rigid-body system. Inverse dynamics is widely used, for example, in the motion control systems or mechanical design of robotic systems.

There are two different approaches described in [14] and [15] for the dynamic modelling of robot manipulators in general: the Newton-Euler approach and the Euler-Lagrange formulation. The second named method treats manipulator as a whole and the dynamic analysis is based on Lagrangian function, which uses the description of both kinetic and potential energy of the system. This formulation provides only the differential equations that determines forces and torques of individual actuators. A result of Newton-Euler approach is a set of dynamic equations, which (besides required forces and torques of actuators) enables to compute the forces and moments acting in the joints. This formulation treats each link of a manipulator separately. It means that the equations describing the linear and angular motion of the links are expressed for each body separately with respect to their body-attached coordinate frames.

Although both of the formulations described above should be equivalent in almost all respects, the Newton-Euler approach appears to be more suitable, intuitive and transparent for open kinematic chains, which is why it will be further used for the purposes of this thesis.

The task of inverse dynamics for respective rigid-body model of a robot manipulator can be summarized by the Equation 4.1.

$$\boldsymbol{\tau} = \mathrm{IDT}(model, \boldsymbol{q}, \dot{\boldsymbol{q}}, \ddot{\boldsymbol{q}}), \tag{4.1}$$

where $\boldsymbol{\tau}$ denotes the vector of generalized forces (torques respectively), *model* describes particular rigid-body system and $\boldsymbol{q}$, $\dot{\boldsymbol{q}}$ and $\ddot{\boldsymbol{q}}$ are vectors of generalized position, velocity and acceleration of the system.

4.2 Newton-Euler Formulation

A method used for analysing of the dynamics of robot manipulators known as the recursive Newton-Euler formulation is described in this section. The more detailed derivation of this formulation is presented in [15] while [16] revises this method from [15] and corrects some notations and formulations. Another detailed explanation can be found in [17].

As described in [14] the inverse dynamics of a open kinematic chain structure can be calculated in the following three steps:

1. Calculate the velocity and the acceleration of each body in the structure.

2. Calculate forces required to produce computed accelerations.

3. Calculate the forces transmitted across the joints from the forces acting on the bodies.

The Newton-Euler method corresponds with these three steps stated above. The approach uses so called forward-backward recursion. The linear and angular motion of individual links in the kinematic chain is determined during the forward recursion. A process starts with link 1 and continues until the last n-th link is reached. The backward recursion then calculates the forces and torques generated by joints, which act on the links. Backward recursion starts at link n and continues to link 1. Since each link is attached to one another at least, the backward recursion considers coupling forces and torques. These quantities describe the influence of forces and torques of the neighbouring links on the current one.

Correctly used method in three-dimensional space returns a vector containing three elements for both forces and torques (together six components). One of these elements describes the actual torque (force respectively), which needs to be generated by the actuator of the robot in order to generate the motion. The five remaining components describe forces and torques acting within the joint (for example on the bearings). This can serve as an useful information, for example, for an estimate of a rate of wear of the robot manipulator.

For the purpose of derivation of the Newton-Euler formulation for an n-link manipulator (completely based on [15]) it is necessary to choose frames $0, \ldots, n$, where frame 0 stands for an inertial frame, and frame i is rigidly attached to link i (as described in [15]). The following list presents several vectors and scalars expressed in frame i, which are required for the Newton-Euler formulation of the equations of motion.

$\boldsymbol{a}_{c,i}$	the acceleration of the center of mass of link i
$\boldsymbol{a}_{e,i}$	the acceleration of the end of link i (i.e. the origin of frame $i+1$)
$\boldsymbol{\omega}_i$	the angular velocity of frame i w.r.t. frame 0
$\boldsymbol{\alpha}_i$	the angular acceleration of frame i w.r.t. frame 0
$\boldsymbol{g}_i$	the acceleration due to gravity expressed in frame i
$\boldsymbol{f}_i$	the force exerted by link $i-1$ on link i
$\boldsymbol{\tau}_i$	the torque exerted by link $i-1$ on link i
$\boldsymbol{R}^i_{i+1}$	the rotation matrix from frame i to frame $i+1$
m_i	the mass of link i
$\boldsymbol{I}_i$	the inertia tensor of link i about a frame parallel to frame i whose origin is at the center of mass of link i
$\boldsymbol{r}_{i,ci}$	the vector from the origin of frame i to the center of mass of link i
$\boldsymbol{r}_{i-1,ci}$	the vector from the origin of frame $i-1$ to the center of mass of link i
$\boldsymbol{r}_{i-1,i}$	the vector from the origin of frame $i-1$ to the origin of frame i
$\boldsymbol{z}_i$	the axis of actuation of frame i w.r.t. frame 0

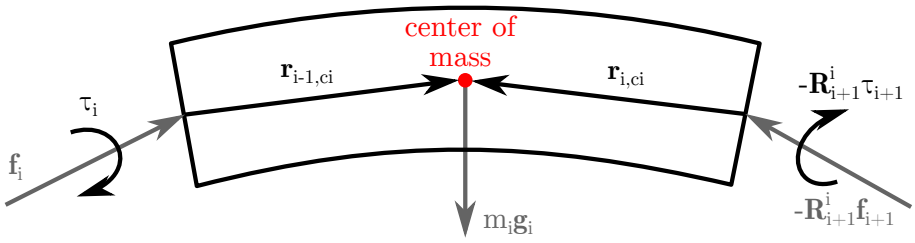

Figure 4.1: Forces and torques acting on link i

Figure 4.1 shows link i together with all forces and torques acting on it. The force exerted by link $i-1$ to link i is denoted as $\boldsymbol{f}_i$. By the law of action and reaction link $i+1$ has to apply a force of $-\boldsymbol{f}_{i+1}$ to link i. Since all the vectors have to be expressed in frame i and the force $-\boldsymbol{f}_{i+1}$ is expressed in frame $i+1$ according to the notation above, it is necessary to multiply it by the rotation matrix $\boldsymbol{R}^i_{i+1}$. The same rule holds for the torques $\boldsymbol{\tau}_i$ and $-\boldsymbol{\tau}_{i+1}$.

The rule, that the rate of change of the linear momentum equals the total force applied to the body, belongs among the facts of Newtonian mechanics. It can be expressed using Equation 4.2.

$$\frac{d(m\boldsymbol{v})}{dt} = \boldsymbol{f}, \tag{4.2}$$

where m is the mass of the body, $\boldsymbol{v}$ is the velocity of the center of mass with respect to an inertial frame, and $\boldsymbol{f}$ is the sum of external forces applied to the body. In case the mass is constant over time (which is the usual case), Equation 4.2 can be simplified to the form of Equation 4.3.

$$m\boldsymbol{a} = \boldsymbol{f}, \tag{4.3}$$

where $\boldsymbol{a} = \dot{\boldsymbol{v}}$ is the acceleration of the center of mass.

Based on Equation 4.2 (4.3 respectively), the force balance equation for link i shown in Figure 4.1 can be written down as

$$\boldsymbol{f}_i - \boldsymbol{R}^i_{i+1}\boldsymbol{f}_{i+1} + m_i\boldsymbol{g}_i = m_i\boldsymbol{a}_{c,i} \tag{4.4}$$

or in a reordered form as

$$\boldsymbol{f}_i = \boldsymbol{R}^i_{i+1}\boldsymbol{f}_{i+1} + m_i\boldsymbol{a}_{c,i} - m_i\boldsymbol{g}_i \tag{4.5}$$

The moment balance equation for link i is computed in the similar way. Two things are important in this case. First, the moment exerted by the force $\boldsymbol{f}$ about a point is given by $\boldsymbol{f} \times \boldsymbol{r}$. The symbol $\boldsymbol{r}$ represents the radial vector from the point where the force is applied to the point about which the moment is computed. Second, the moment balance equation does not contain the vector $m_i\boldsymbol{g}_i$, since it is applied directly at the center of mass (see Equation 4.4). The moment balance equation has a form

$$\boldsymbol{\tau}_i - \boldsymbol{R}^i_{i+1}\boldsymbol{\tau}_{i+1} + \boldsymbol{f}_i \times \boldsymbol{r}_{i-1,ci} - (\boldsymbol{R}^i_{i+1}\boldsymbol{f}_{i+1}) \times \boldsymbol{r}_{i,ci} = \boldsymbol{I}_i\boldsymbol{\alpha}_i + \boldsymbol{\omega}_i \times (\boldsymbol{I}_i\boldsymbol{\omega}_i) \tag{4.6}$$

which can be reordered to the form

$$\boldsymbol{\tau}_i = \boldsymbol{R}^i_{i+1}\boldsymbol{\tau}_{i+1} - \boldsymbol{f}_i \times \boldsymbol{r}_{i-1,ci} + (\boldsymbol{R}^i_{i+1}\boldsymbol{f}_{i+1}) \times \boldsymbol{r}_{i,ci} + \boldsymbol{I}_i\boldsymbol{\alpha}_i + \boldsymbol{\omega}_i \times (\boldsymbol{I}_i\boldsymbol{\omega}_i) \tag{4.7}$$

Both the moment balance equation 4.6 and the force balance equation 4.4 are parts of the backward recursion of the Newton-Euler algorithm. Terms $\boldsymbol{a}_{c,i}$, $\boldsymbol{\alpha}_i$ and $\boldsymbol{\omega}_i$ have to be expressed by the use of the vectors of generalized position $\boldsymbol{q}$, velocity $\dot{\boldsymbol{q}}$ and acceleration $\ddot{\boldsymbol{q}}$ as the next step in order to obtain the solution of inverse dynamic task in form of Equation 4.1. The relation between these quantities is found within the forward recursion of the algorithm.

The angular velocity of a frame i expressed in the inertial frame (0) can be written as Equation 4.8.

$$\boldsymbol{\omega}^{(0)}_i = \boldsymbol{\omega}^{(0)}_{i-1} + \boldsymbol{z}_{i-1}\dot{\boldsymbol{q}}_i \tag{4.8}$$

Previous relation can be recomputed into the frame i using the transformation matrix $\boldsymbol{R}^{i-1}_i$, which results in

$$\boldsymbol{\omega}_i = (\boldsymbol{R}^{i-1}_i)^T\boldsymbol{\omega}_{i-1} + \boldsymbol{b}_i\dot{\boldsymbol{q}}_i \tag{4.9}$$

where

$$\boldsymbol{b}_i = (\boldsymbol{R}^0_i)^T\boldsymbol{R}^0_{i-1}\boldsymbol{z}_0 \tag{4.10}$$

is the axis of rotation of joint i expressed in frame i.

The angular acceleration of link i in the coordinate frame of link i is described as

$$\boldsymbol{\alpha}_i = (\boldsymbol{R}^0_i)^T\dot{\boldsymbol{\omega}}^{(0)}_i \tag{4.11}$$

where $\dot{\boldsymbol{\omega}}^{(0)}_i$ is the time derivative of Equation 4.8

$$\dot{\boldsymbol{\omega}}_i^{(0)} = \dot{\boldsymbol{\omega}}_{i-1}^{(0)} + \boldsymbol{z}_{i-1}\ddot{\boldsymbol{q}}_i + \boldsymbol{\omega}_i^{(0)} \times \boldsymbol{z}_{i-1}\dot{\boldsymbol{q}}_i \tag{4.12}$$

which can be recomputed into the angular acceleration expressed in the coordinate frame of i-th link as follows

$$\boldsymbol{\alpha}_i = (\boldsymbol{R}_i^{i-1})^T\boldsymbol{\alpha}_{i-1} + \boldsymbol{b}_i\ddot{\boldsymbol{q}}_i + \boldsymbol{\omega}_i \times \boldsymbol{b}_i\dot{\boldsymbol{q}}_i \tag{4.13}$$

The linear velocity of the center of mass has to be expressed in order to obtain the linear acceleration as its time derivative.

$$\boldsymbol{v}_{c,i}^{(0)} = \boldsymbol{v}_{e,i-1}^{(0)} + \boldsymbol{\omega}_i^{(0)} \times \boldsymbol{r}_{i-1,ci}^{(0)} \tag{4.14}$$

$$\boldsymbol{a}_{c,i}^{(0)} = \boldsymbol{a}_{e,i-1}^{(0)} + \dot{\boldsymbol{\omega}}_i^{(0)} \times \boldsymbol{r}_{i-1,ci}^{(0)} + \boldsymbol{\omega}_i^{(0)} \times (\boldsymbol{\omega}_i^{(0)} \times \boldsymbol{r}_{i-1,ci}^{(0)}) \tag{4.15}$$

$$\boldsymbol{a}_{c,i} = (\boldsymbol{R}_i^0)^T\boldsymbol{a}_{c,i}^{(0)} \tag{4.16}$$

As the cross product is invariable with respect to the rotations about the axis defined by $\boldsymbol{a} \times \boldsymbol{b}$, one can apply Equation 4.17 on the expression 4.16.

$$\boldsymbol{R}(\boldsymbol{a} \times \boldsymbol{b}) = (\boldsymbol{R}\boldsymbol{a}) \times (\boldsymbol{R}\boldsymbol{b}) \tag{4.17}$$

$$\boldsymbol{a}_{c,i} = (\boldsymbol{R}_i^{i-1})^T\boldsymbol{a}_{e,i-1} + \dot{\boldsymbol{\omega}}_i \times \boldsymbol{r}_{i-1,ci} + \boldsymbol{\omega}_i \times (\boldsymbol{\omega}_i \times \boldsymbol{r}_{i-1,ci}) \tag{4.18}$$

The acceleration of the end of a link i can be found simply by replacing of $\boldsymbol{r}_{i-1,ci}$ by $\boldsymbol{r}_{i-1,i}$.

$$\boldsymbol{a}_{e,i} = (\boldsymbol{R}_i^{i-1})^T\boldsymbol{a}_{e,i-1} + \dot{\boldsymbol{\omega}}_i \times \boldsymbol{r}_{i-1,i} + \boldsymbol{\omega}_i \times (\boldsymbol{\omega}_i \times \boldsymbol{r}_{i-1,i}) \tag{4.19}$$

Now, all the terms $\boldsymbol{a}_{c,i}$, $\boldsymbol{\alpha}_i$ and $\boldsymbol{\omega}_i$ have been described with dependence on quantities $\boldsymbol{q}$, $\dot{\boldsymbol{q}}$ and $\ddot{\boldsymbol{q}}$. The forward-backward recursion of the Newton-Euler algorithm can be performed as follows:

1. **Forward recursion**
   Start the algorithm with the initial conditions

   $$\boldsymbol{\omega}_0 = 0, \qquad \boldsymbol{\alpha}_0 = 0, \qquad \boldsymbol{a}_{c,0} = 0, \qquad \boldsymbol{a}_{e,0} = 0 \tag{4.20}$$

   and get values $\boldsymbol{\omega}_i$, $\boldsymbol{\alpha}_i$, $\boldsymbol{a}_{c,i}$, $\boldsymbol{a}_{e,i}$ by solving Equations 4.9, 4.13, 4.19 and 4.18 (in that order) for each link i starting from $i = 1$ to n.

2. **Backward recursion**
   Start with terminal conditions

   $$\boldsymbol{f}_{n+1} = \boldsymbol{f}_{ext}, \qquad \boldsymbol{\tau}_{n+1} = \boldsymbol{\tau}_{ext} \tag{4.21}$$

   where $\boldsymbol{f}_{ext}$ and $\boldsymbol{\tau}_{ext}$ are the external forces acting on the manipulator and compute $\boldsymbol{f}_{n+1}$ and $\boldsymbol{\tau}_{n+1}$ by solving Equations 4.5 and 4.7 (in that order) for each link i starting from $i = n$ to 1.

Note, that the formulation described above holds only for a robot manipulator with revolute joints. Equations 4.9, 4.13, 4.18 and 4.19 have to be modified into a slightly different form in order to deploy this formulation in a system with some prismatic joints.

An example of the use of the Newton-Euler formulation in order to solve an actual dynamic problem related to this thesis is shown in Section 4.4. An illustrative example of design of the dynamic model using this approach for a simple planar manipulator can be found in [15]. Another example containing detailed description of use of this method for a six-axis manipulator is included in [16].

4.3 Gyroscopic Effect

Proposed technology of grinding produces a gyroscopic effect. Quickly rotating grinding disc with the other rotating masses (the shaft or the rotor of the grinding tool) mounted on the flange of the robot can be considered as a flywheel. This flywheel moves along the circular trajectories in some phases during the grinding of the billet (during the entire movement in case of the billet with circular section or at the corners in case of the billet with the quadratic section). It means that the flywheel rotates around two axes. The forced rotation of the flywheel in the fixed frame produces gyroscopic effect, which can have the negative influence on the system. An excessive mechanical stress and wear of even a damage of a robot manipulator can be caused by the influence of this effect.

As the detailed derivation of this problem is not elementary and it is not the main topic of this thesis, its concept is simplified for further purposes and illustrated in Figure 4.2.

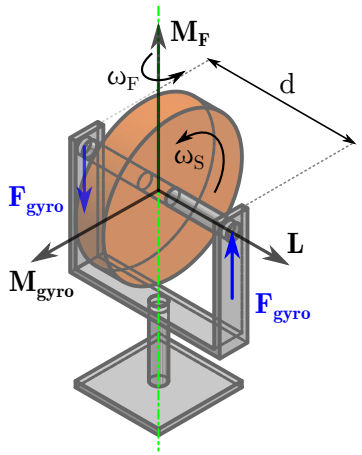

Figure 4.2: Flywheel in a gimbals

From the physical point of view, this problem can by described as a heavy flywheel rotating around its axis of symmetry in the fixed frame. The moment of inertia with respect to this axis of rotation is denoted as J. There is an angular momentum $\boldsymbol{L}$ of the spin of the flywheel in the axis of rotation. Then, there is an external force around an axis acting on this flywheel. The external force generates a forced moment $\boldsymbol{M}_{\mathrm{F}}$. Due to the influence of this moment, a precession movement caused by a gyroscopic moment $\boldsymbol{M}_{\mathrm{gyro}}$ arises. The movement forces the spin axis of the flywheel to rotate into the direction of the axis of forced rotation. As informally (but illustratively) described in [18], *the vector of angular momentum is trying to chase the vector of the forced torque.*

As a further simplification let's assume, that the axis of forced rotation is perpendicular to the spin axis of the flywheel, which is also the case of the grinding tool. As the flywheel with the angular momentum $\boldsymbol{L}$ is mounted into a fixed frame, it can not perform the precession movement, i.e. the axis of the angular momentum cannot rotate into the direction of the axis of $\boldsymbol{M}_{\mathrm{F}}$ (axis of forced rotation), which would be the case of free flywheel.

According to [19], the magnitude of the generated moment of gyroscopic precession can be computed as

$$M_{\mathrm{gyro}} = J\omega_{\mathrm{S}}\omega_{\mathrm{F}} \tag{4.22}$$

where J represents the moment of inertia of the flywheel, ω_{S} denotes the angular velocity of the spinning flywheel and ω_{F} stands for the angular velocity of the forced rotation. The moment of gyroscopic precession generates the forces acting on the bearings of the spin axis of the flywheel. The magnitude of these forces can be computed as

$$F_{\mathrm{gyro}} = (J\omega_{\mathrm{S}}\omega_{\mathrm{F}})/d \tag{4.23}$$

where the meaning of the symbols is the same as in Equation 4.22 and d denotes the distance between bearings at the end of the axis of spinning flywheel. These are the forces, which cause the mechanical stress in the bearings and increase their wear.

4.4 Example Using Newton-Euler Approach

It will be shown how to use the Newton-Euler formulation for design of a dynamic model of gyroscope flywheel in the gimbals in the following example based on [20]. Let's consider the flywheel in the gimbals shown in Figure 4.3.

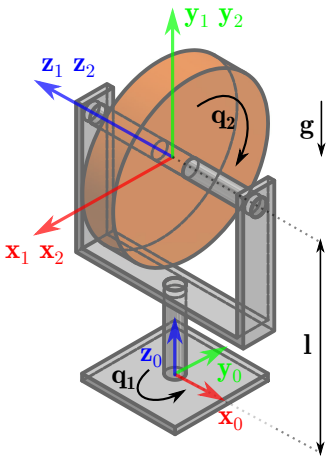

Figure 4.3: Flywheel in a gimbals (example)

This system consists of three links (base, gimbals and flywheel) connected together by two revolute joints. There is a coordinate frame attached to each body, which will be used to express the dynamic behaviour using the Newton-Euler method. There is the fixed base frame $[x_0, y_0, z_0]$, the frame $[x_1, y_1, z_1]$ attached to the gimbals and the frame $[x_2, y_2, z_2]$ connected with the flywheel in its origin. The origins of frames 1 and 2 are identical, but they are coupled to the different bodies. The frames are attached according to Denavit-Hartenberg notation as

it would be done in case of modelling of a serial robot manipulator. However, this is not really important in this case. An arbitrary chosen coordinate frames can be attached to the individual bodies. The important thing is to express the relations between each two of them correctly.

To simplify the computation and to emphasise the influence of the gyroscopic effect let's assume that the mass and the moment of inertia of the gimbals are equal zero and that the center of mass of flywheel is aligned with the origin of the gimbals.

Following parameters (denoted according the Section 4.2) of the system are known:

$$\boldsymbol{r}_{0,1} = \begin{bmatrix}0\\ l\\ 0\end{bmatrix}, \quad \boldsymbol{r}_{1,2} = \begin{bmatrix}0\\ 0\\ 0\end{bmatrix}, \quad \boldsymbol{r}_{0,c1} = \begin{bmatrix}0\\ 0\\ 0\end{bmatrix}, \quad \boldsymbol{r}_{1,c2} = \begin{bmatrix}0\\ 0\\ 0\end{bmatrix}, \quad \boldsymbol{r}_{1,c1} = \begin{bmatrix}0\\ 0\\ 0\end{bmatrix}, \quad \boldsymbol{r}_{2,c2} = \begin{bmatrix}0\\ 0\\ 0\end{bmatrix} \tag{4.24}$$

$$\boldsymbol{R}_1^0 = \begin{bmatrix}\sin q_1 & 0 & -\cos q_1\\ -\cos q_1 & 0 & -\sin q_1\\ 0 & 1 & 0\end{bmatrix} \qquad \boldsymbol{R}_2^1 = \begin{bmatrix}\cos q_2 & -\sin q_2 & 0\\ \sin q_2 & \cos q_2 & 0\\ 0 & 0 & 1\end{bmatrix} \tag{4.25}$$

$$\boldsymbol{I}_1 = \boldsymbol{0} \qquad \boldsymbol{I}_2 = \begin{bmatrix}\frac{1}{12}m_2(3R^2+h^2) & 0 & 0\\ 0 & \frac{1}{12}m_2(3R^2+h^2) & 0\\ 0 & 0 & \frac{1}{2}m_2R^2\end{bmatrix} \tag{4.26}$$

$$\boldsymbol{z}_0 = [0,0,1]^T \qquad \boldsymbol{g}_i = (\boldsymbol{R}_i^0)^T\boldsymbol{g}_0 \qquad \boldsymbol{g}_0 = [0,0,-g]^T \tag{4.27}$$

Mass of the first link is equal zero and the mass of second one is denoted as m_2. Parameter R in the matrix $\boldsymbol{I}_2$ denotes the radius of the flywheel while h stands for its thickness. There are no external forces acting on the system, thus $\boldsymbol{f}_{ext} = \boldsymbol{0}$ and $\boldsymbol{\tau}_{ext} = \boldsymbol{0}$. Parameters use quantities q_1 and q_2, which describe the orientation of the frame (gimbals) and the orientation of the flywheel as shown in Figure 4.3. Once all the parameters for the Newton-Euler formulation are known, the forward-backward recursion over each link in the system can be performed.

Forward recursion Link 1

$$\boldsymbol{\omega}_1 = \begin{bmatrix}0\\ \dot{q}_1\\ 0\end{bmatrix} \qquad \boldsymbol{\alpha}_1 = \begin{bmatrix}0\\ \ddot{q}_1\\ 0\end{bmatrix} \qquad \boldsymbol{a}_{e,1} = \begin{bmatrix}0\\ 0\\ 0\end{bmatrix} \qquad \boldsymbol{a}_{c,1} = \begin{bmatrix}0\\ 0\\ 0\end{bmatrix} \tag{4.28}$$

Forward recursion Link 2

$$\boldsymbol{\omega}_2 = \begin{bmatrix}\dot{q}_1\sin q_2\\ \dot{q}_1\cos q_2\\ \dot{q}_2\end{bmatrix} \qquad \boldsymbol{\alpha}_2 = \begin{bmatrix}\ddot{q}_1\sin q_2 + \dot{q}_1\dot{q}_2\cos q_2\\ \ddot{q}_1\cos q_2 - \dot{q}_1\dot{q}_2\sin q_2\\ \ddot{q}_2\end{bmatrix} \qquad \boldsymbol{a}_{e,2} = \begin{bmatrix}0\\ 0\\ 0\end{bmatrix} \qquad \boldsymbol{a}_{c,2} = \begin{bmatrix}0\\ 0\\ 0\end{bmatrix} \tag{4.29}$$

Backward recursion Link 2

$$\boldsymbol{f}_2 = \begin{bmatrix}m_2g\sin q_2\\ m_2g\cos q_2\\ 0\end{bmatrix} \qquad \boldsymbol{\tau}_2 = \begin{bmatrix}\frac{1}{2}m_2R^2\dot{q}_1\dot{q}_2\cos q_2 + \frac{1}{12}m_2(3R^2+h^2)\ddot{q}_1\sin q_2\\ -\frac{1}{2}m_2R^2\dot{q}_1\dot{q}_2\sin q_2 + \frac{1}{12}m_2(3R^2+h^2)\ddot{q}_1\cos q_2\\ \frac{1}{2}m_2R^2\ddot{q}_2\end{bmatrix} \tag{4.30}$$

Backward recursion Link 1

$$\boldsymbol{f}_1 = \begin{bmatrix} 0 \\ (m_1 + m_2)g \\ 0 \end{bmatrix} \qquad \boldsymbol{\tau}_1 = \begin{bmatrix} \frac{1}{2}m_2R^2\dot{q}_1\dot{q}_2 \\ \frac{1}{12}m_2(3R^2 + h^2)\ddot{q}_1 \\ \frac{1}{2}m_2R^2\ddot{q}_2 \end{bmatrix} \tag{4.31}$$

Several observations can be done from these results. Obviously, the torque exerted on the axis z_2 depends only on the angular acceleration around this axis (and on the dynamic parameters of course). A non-intuitive fact is, that torque exerted on the axis y_1 does not depend on the rotational speed of the flywheel at all. Again, only the angular acceleration around this axis influences the resulting torque in this direction.

The torque of gyroscopic precession, which forces the flywheel to align its spin axis with the axis of forced torque, appears in direction of the axis x_1. One can see from the results of Newton-Euler algorithm, that this torque depends on the inertial parameters of the flywheel and on the rotational velocities of both links. However, the flywheel cannot rotate around the axis x_1 in this case, because it is fixed in the frame. Instead of it, the forces exerted on the bearings of the flywheel axis appear.

5 Simulations

Dynamic simulations of the robot manipulator introduced in previous text are described in this chapter. The main goal of simulations is to investigate the suitability of the proposed industrial manipulator for the described task. The implemented simulation tool should be able to determine the influence of torque generated by gyroscopic precession on the system. An expected result of the dynamic simulation is a discussion whether the robot is capable to perform grinding operation with proposed grinding tool or not. The entire simulation tool has been developed in the MATLAB environment with the support of some external scripts and libraries.

5.1 Simulation Set-up

Let's consider completely free robot workspace with the billet to be ground as pictured in Figure 5.1. The body of the billet is located in the positive direction of y-axis of the world coordinate frame in such a way that the center of the face of the billet is located in the position $[0, 0, z]^T$ of the world coordinate frame. The billet lays on a production line which occupies the entire half-plane in direction of the positive part of y-axis. Hence, the manipulator should be situated into the negative half-plane of the y-axis. The robot manipulator KUKA KR 500 R2830 MT, introduced in Chapter 3, is used in the simulations. The manipulator is equipped with a grinding tool which has been described in Section 3.3. There are supposed to be further devices in the robot workspace in the real industrial application, such as a stock stop for incoming billets or ground material exhaustion. However, none of this accessories is considered in the workspace during the simulation.

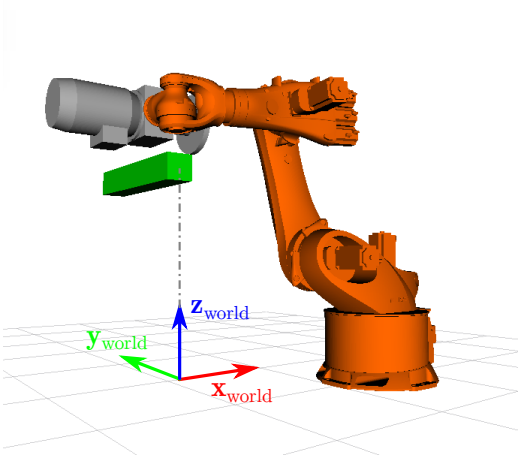

Figure 5.1: Robot workspace in simulator

The simulation procedure consists of several steps. Firstly, a trajectory of the grinding tool is found which leads to a required machining of a billet and to smooth movement of the manipulator. Secondly, corresponding joint trajectories are found using the analytical inverse kinematic task. Finally, the inverse dynamic task based on Newton-Euler approach is deployed to obtain torques, which have to be generated by actuators of the robot.

5.2 Trajectory Generation

A problem of the trajectory planning is separated into two subtasks, as already mentioned in the previous text. The first one is to find a trajectory for the reference point at the circumference of the grinding disc (see Section 3.3). This information allows to compute corresponding trajectory of the grinding tool and of the flange of the robot manipulator. Note that the flange trajectory, which has been found, contains both position and orientation of the corresponding coordinate frame. The second task is then the computation of inverse kinematics for the manipulator. The motion of the entire robot manipulator is based on a motion of the grinding tool (grinding disc respectively) therefore the trajectory of the grinding tool has to be found first. Then, based on this information, the motion of the manipulator (i.e. joint trajectories) can be found.

The grinding of a billet with a quadratic cross section appears to be more complex task than the machining of the one, whose cross section is circular. The reason is that two different types of the grinding tool motion have to be used during this operation: a linear movement along the edge of the billet and the rotational movement which aligns the spindle axis parallel to the following perpendicular edge at the corner.

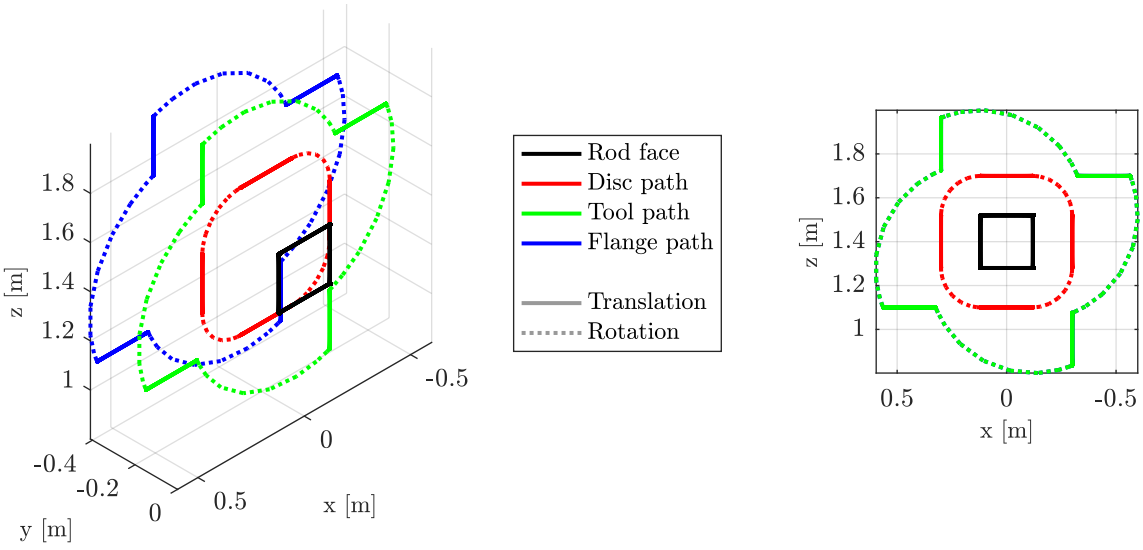

(a) 3D view

(b) Front view

Figure 5.2: Grinding tool trajectory

Let's consider the billet with quadratic cross-section with the edge of length 240 mm. A grinding angle is defined as an angle between the plane of the face of a billet and the plane defined by the position of the contact point and the axis of rotation of the grinding disc. The required grinding angle can be different according to the customer specification. The angle of

$\frac{\pi}{4}$ has been chosen for the simulation purposes. The bottom side of the billet is placed on a production line 1280 mm above the ground. It corresponds to the distance of 1280 mm in the positive direction of z-axis in the world coordinate frame (see 5.1). The billet itself and the production line are situated in the positive direction of y-axis hence the negative part of the y-axis is meant to be a workspace of the robot manipulator.

The velocity of the grinding tool is the next parameter, which has to be set in order to compute the trajectories. There are several factors which have a significant influence on the speed of machining. These are, for example, ground material and its allowed heating temperature or material of used grinding disc [21]. The required time for machining of one edge has been set to 4 seconds (based on a size of considered billet). Time required for the rotation of the grinding tool about 90 degrees at the corner has to take into account the gyroscopic effect which needs to be compensated by actuators of the robot. The amount of material which has to be machined at the corner is quite small. From this matter of perspective, the speed of the rotation of the tool could correspond to the maximum speed, which is the manipulator able to move with. However, the faster the change is, the bigger torque caused by gyroscopic precession is produced and the bigger torque has to be compensated by the actuators of the manipulator. Time for the rotation at the corner has been set to 3 seconds. This value is based on a rough estimate of precession torque and on torques limits which describe the torque that the manipulator is able to compensate permanently.

The trajectory for the reference point on the grinding disc can be divided into eight segments (4 translational and 4 rotational) around the entire billet face as drawn in Figure 5.2. The motion profile for each segment is generated and these motion profiles are then merged to the required trajectory. Once the trajectory for the reference point is found, it is easy to compute position and orientation of the flange of the robot manipulator using space transformation matrices. The inverse kinematic task can be solved as a next step.

Motion Profile

It is obvious that the grinding tool executes either translational and rotational movement separately (in case of the billet with quadratic section) or a combination of these two movements in the same time (in case of circular cross section). In both cases the implemented solution for the generating of motion profile executes point-to-point (rest-to-rest) trajectory.

A typical requirement related to the motion in industrial automation is a bounded jerk. The jerk describes the rate of change of acceleration. A limitation of this quantity reduces stress induced in actuators and structure of the manipulator as well as wear of the entire device.

To fulfil the requirement of bounded jerk a simple method using two third-order polynomials to describe a velocity profile has been implemented. Given the initial, end and maximum velocity and acceleration, required time and distance and the direction of movement the motion profile can be created. This approach results into two fourth-order polynomials describing the trajectory. The entire movement is divided into three phases: acceleration phase, plane phase and deceleration phase. The maximum velocity is reached during the acceleration phase, it is preserved during the plane phase and later it is decreased to zero during the deceleration. Equations 5.1 and 5.2 allow to determine the coefficients c_{ai}, c_{p0}, c_{di}. The position can be computed as a finite integral over time and the jerk is the time derivative of acceleration.

$$v(t) = \begin{cases} c_{a3}t^3 + c_{a2}t^2 + c_{a1}t + c_{a0} & \text{acceleration phase} \\ c_{p0} & \text{plane phase} \\ c_{d3}t^3 + c_{d2}t^2 + c_{d1}t + c_{d0} & \text{decceleration phase} \end{cases} \tag{5.1}$$

$$a(t) = \dot{v}(t) = \begin{cases} 3c_{a3}t^2 + 2c_{a2}t + c_{a1} & \text{acceleration phase} \\ 0 & \text{plane phase} \\ 3c_{d3}t^2 + 2c_{d2}t + c_{d1} & \text{decceleration phase} \end{cases} \tag{5.2}$$

The motion profile for rotational movement about 360 degrees starting in position -180 deg with zero initial and end velocity and acceleration can be seen in Figure 5.3. Required time has been set to 2.0 s, maximum velocity to 400 deg/s and maximum acceleration to 550 deg/s^2.

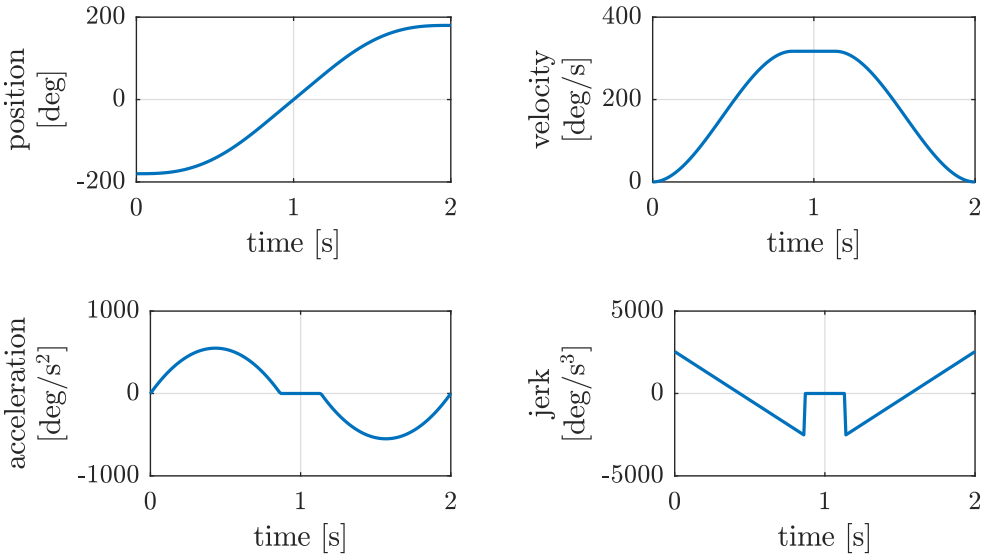

Figure 5.3: Motion profile

5.3 Planning Joint Trajectories

So far, the trajectory for the grinding tool has been created. The following step is to compute joint trajectories of manipulator itself based on the trajectory of the end-effector. As mentioned before, computed end-effector trajectory contains both position and orientation information. Using the analytic solution of the inverse kinematic task, one can obtain joint coordinates for each position of grinding tool trajectory. As the trajectory is sampled with fixed time step, it is easy to compute corresponding velocity and acceleration of each joint for each time instant. A situation may occur when the trajectory computed by inverse kinematic task contains a configuration change of the manipulator during two consecutive time steps. This leads to a step change in joint coordinates and to the spikes in corresponding velocity graph. A function has been implemented, which provides a check of maximum allowed velocity according to the manufacturer documentation in order to suppress these unacceptable solutions. An example of computed joint trajectories, velocities and accelerations for robot manipulator in position $[1.5, -1.0, -0.5]^T$ m in the world coordinate frame grinding a billet placed 1280 mm above the ground (see 5.1) is shown in Figures 5.4, 5.5 and 5.6.

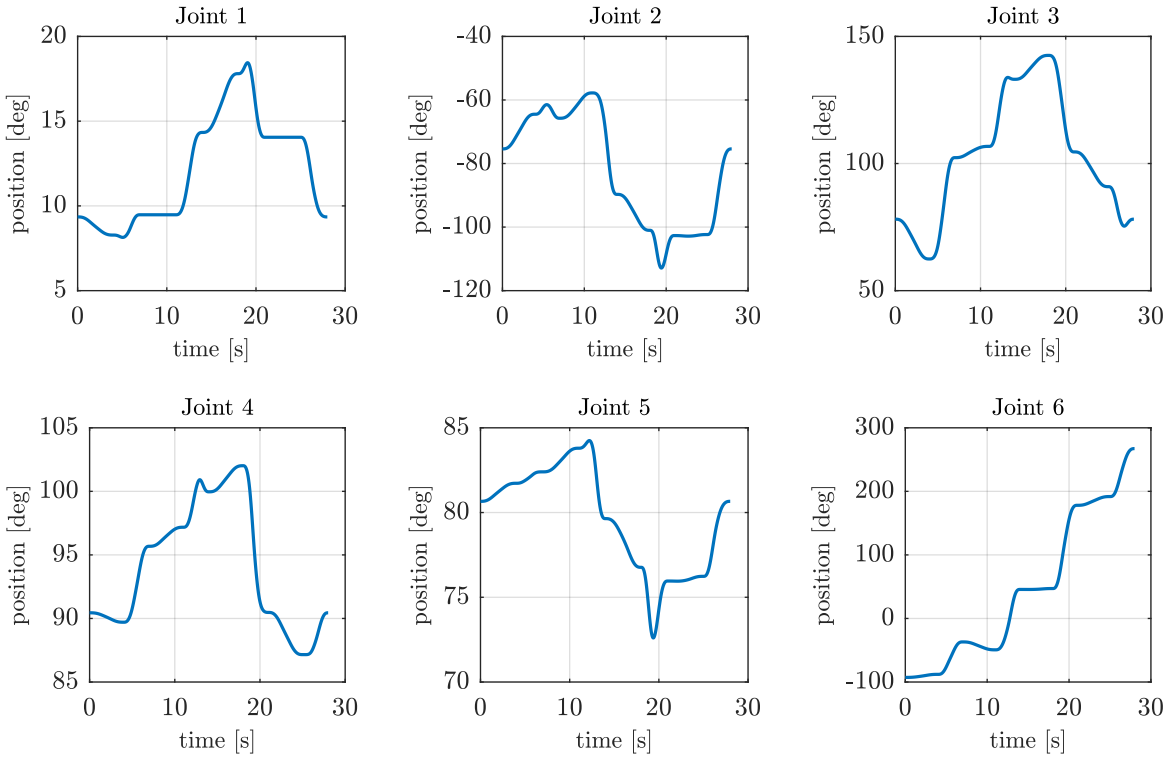

Figure 5.4: Joint coordinates during the grinding of a billet

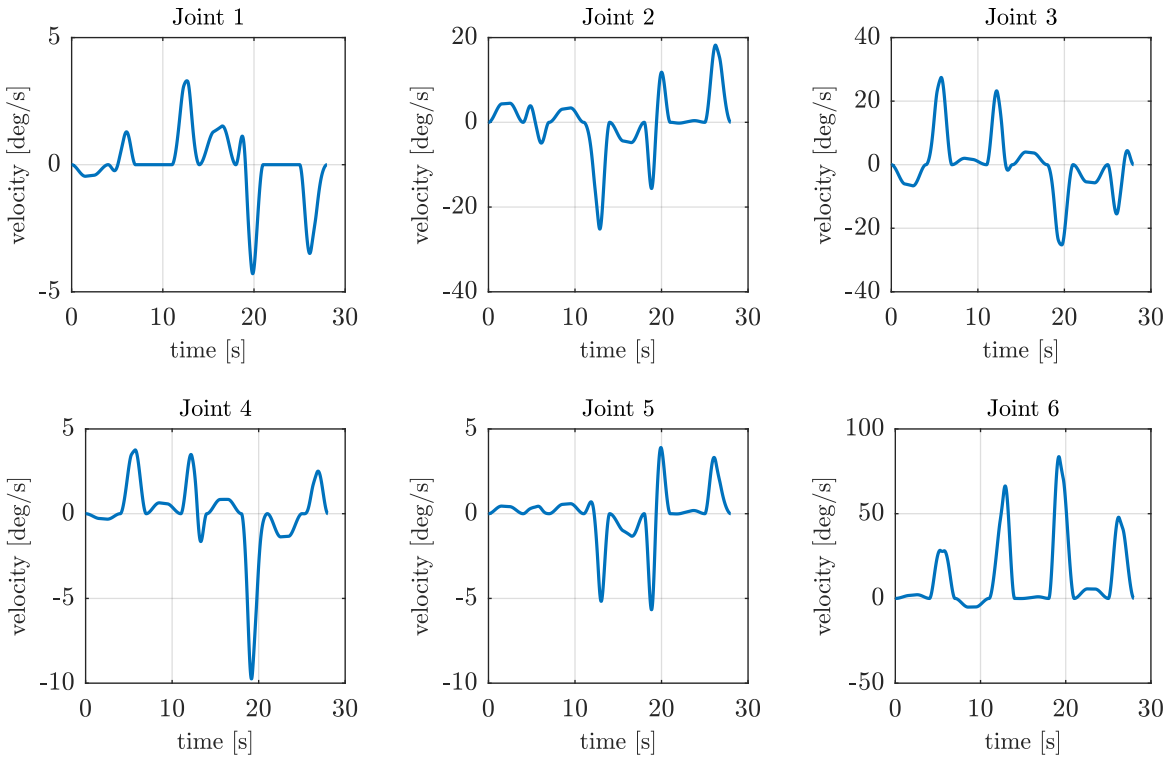

Figure 5.5: Joint velocities during the grinding of a billet

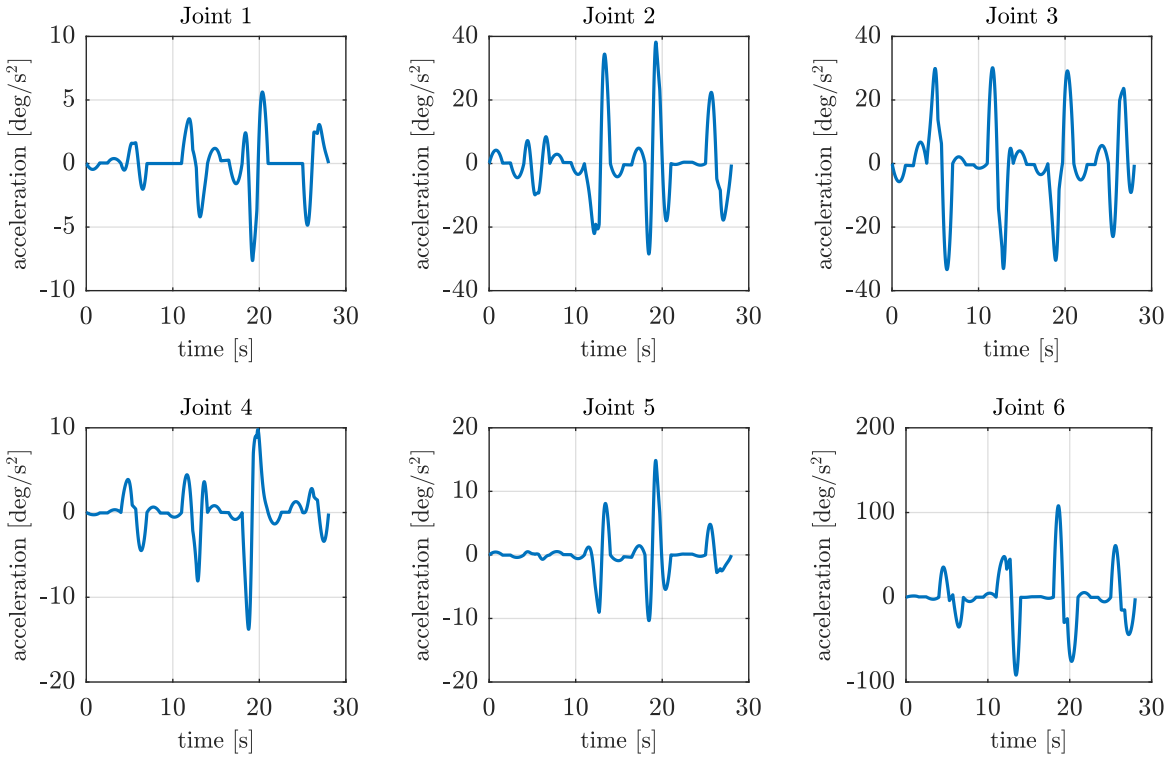

Figure 5.6: Joint accelerations during the grinding of a billet

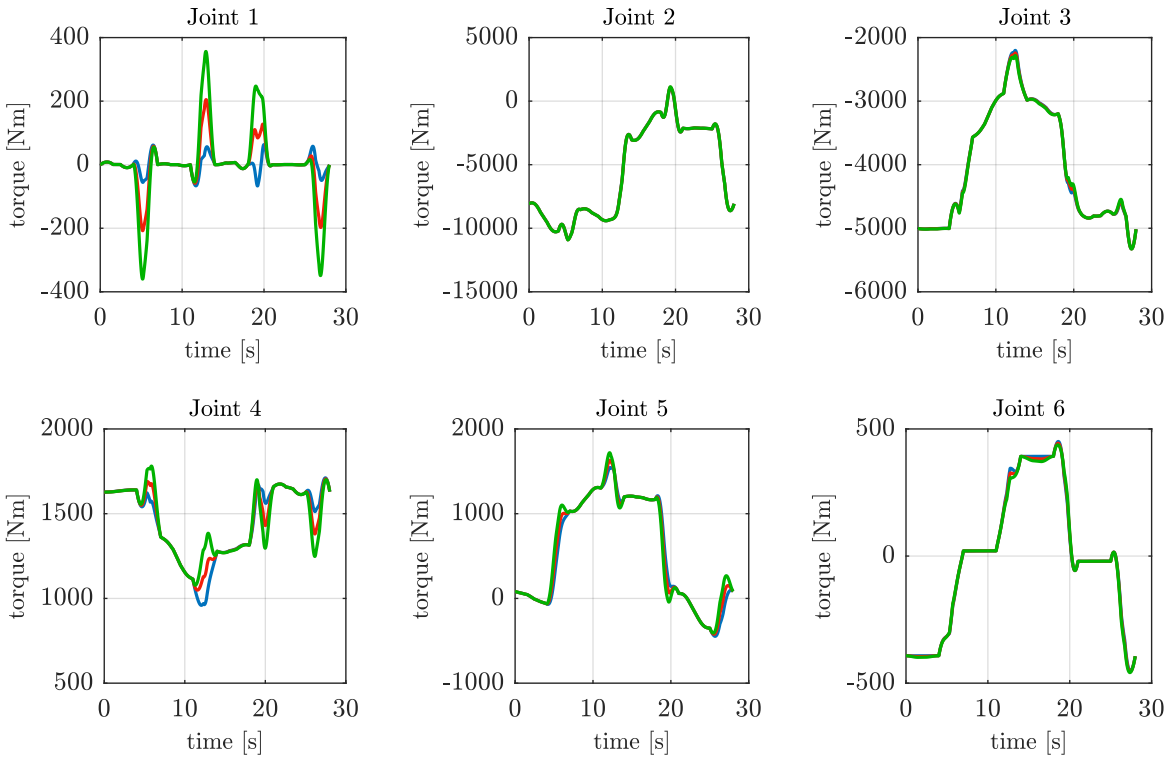

Figure 5.7: Joint torques for different speeds of the grinding disc: **0**, **1500**, **3000** rpm

5.4 Inverse Dynamics Solution

The solution of the inverse dynamic task is entirely based on the Recursive Newton-Euler Algorithm described in Section 4.2. The solution is obtained according to the symbolic expression described in Equation 4.1. Computed joint coordinates, velocities and acceleration together with a description of respective robot manipulator are processed by the function which provides a solution of the Recursive Newton-Euler Algorithm. An output of this function is a set of torques in individual joints (axes) in each time instant of the movement. Such a solution is shown in Figure 5.7.

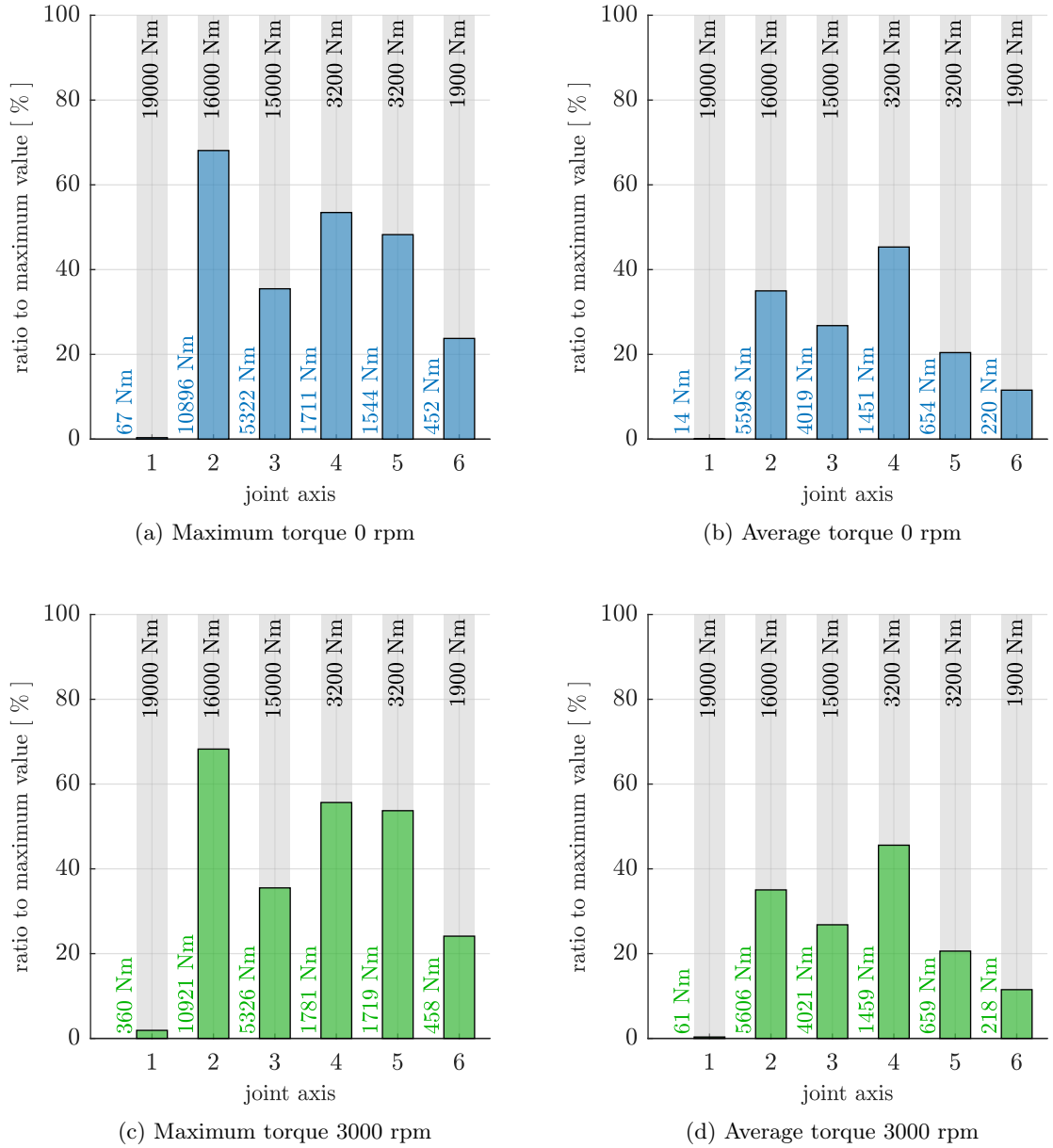

(a) Maximum torque 0 rpm

(b) Average torque 0 rpm

(c) Maximum torque 3000 rpm

(d) Average torque 3000 rpm

Figure 5.8: Ratio of reached torques

Computed torques have to respect limits of process forces. These are external forces with an influence on the robot. The maximum process forces depend on several factors such as the

position of the robot or its payload. The process force limit of each robot axis is specified by manufacturer. These values specify the limited torque, which is able to be compensated permanently by the robot. Figure 5.8 shows the bar graphs, which express the ratio of maximum reached torque to maximum allowed value as well as the ratio of the average torque to the maximum one. The load of each joint, which must not be exceeded, is considered to be 100% in the bar graphs. An exact value specified by robot manufacturer is shown at the top of each bar.

It is reasonable to keep maximal torques produced by joint actuators as low as possible. Low values of torque saves energy consumption and reduces mechanical stress and wear of the actuators. There is a simple position optimisation method (discussed in Section 5.8), which searches for suitable positions of the robot manipulator according to the requirement to keep the torques as low as possible.

5.5 Torque Graph Analysis

Although it is quite difficult to describe exact influence of all individual forces and torques acting in such a complex system as the six axis manipulator is, it is still possible to see some significant features.

The details of graphs of torques generated by joints 1, 5 and 6 are shown in Figure 5.9. Figures containing a proof of the influence of gyroscopic effect have been chosen for the analysis. The regions highlighted with grey color represents time intervals during which the manipulator rotates the grinding tool at the corner of the billet. The duration of each of these intervals is exactly 3 seconds. The sixth joint generates the torque which forces the flywheel (grinding disc) to rotate. As follows on from Section 4.3, the most significant influence of the gyroscopic precession can be observed in these joints of manipulator, whose axis of rotation lays in the plane perpendicular to the axis of forced rotation of the flywheel. The second important factor is the rate of parallelism of the axis of gyroscopic precession and the axis of rotation of particular joint. The axis of joint 5 is located in the plane, whose normal is created by the aforementioned sixth axis, and the axis of joint 1 one lays once again in another plane perpendicular to the axis of the sixth joint. Other joint axes are influenced by torque generated by gyroscopic precession as well, and the same rule holds for them as will be described for joints 1, 5 and 6 in following paragraph.

Let's investigate individual time intervals of the entire movement of the grinding tool around the face of the billet from Figure 5.9. The manipulator is grinding the edges of the billet face during the time intervals $[0, 4]$, $[7, 11]$, $[14, 18]$ and $[21, 25]$. As the translational movement is quite slow (240 mm per 4 seconds) during this operation and there is no need to rotate with the grinding tool about large angle, the torques of actuators for different grinding speeds of the disc do not differ significantly. The actuators compensate mainly the weight of following links during these time intervals and the rotational speed of the grinding disc has no significant influence on the actuators. The exception is the torque in the axis 6 in time interval $[14, 18]$ s. Apparently, sum of the movements of other axes creates the forced torque acting on the grinding disc, hence a gyroscopic moment, which needs to be compensated by change of the torque exerted by the sixth axis, appears. This can be easily demonstrated by a simulation where the manipulator is placed to the position $[-2.0, -0.7, -0.5]^T$ m in the world coordinate frame. Grinding of the same billet on the same position as in the previous case is then executed. The robot is able to execute grinding trajectory using only joints 2, 3 and 6. As all moving joint axis are in all cases parallel to the axis of forced moment on the grinding disc, any difference for individual grinding speed in sixth joint torque will be observed. Similar behaviour can be observed in

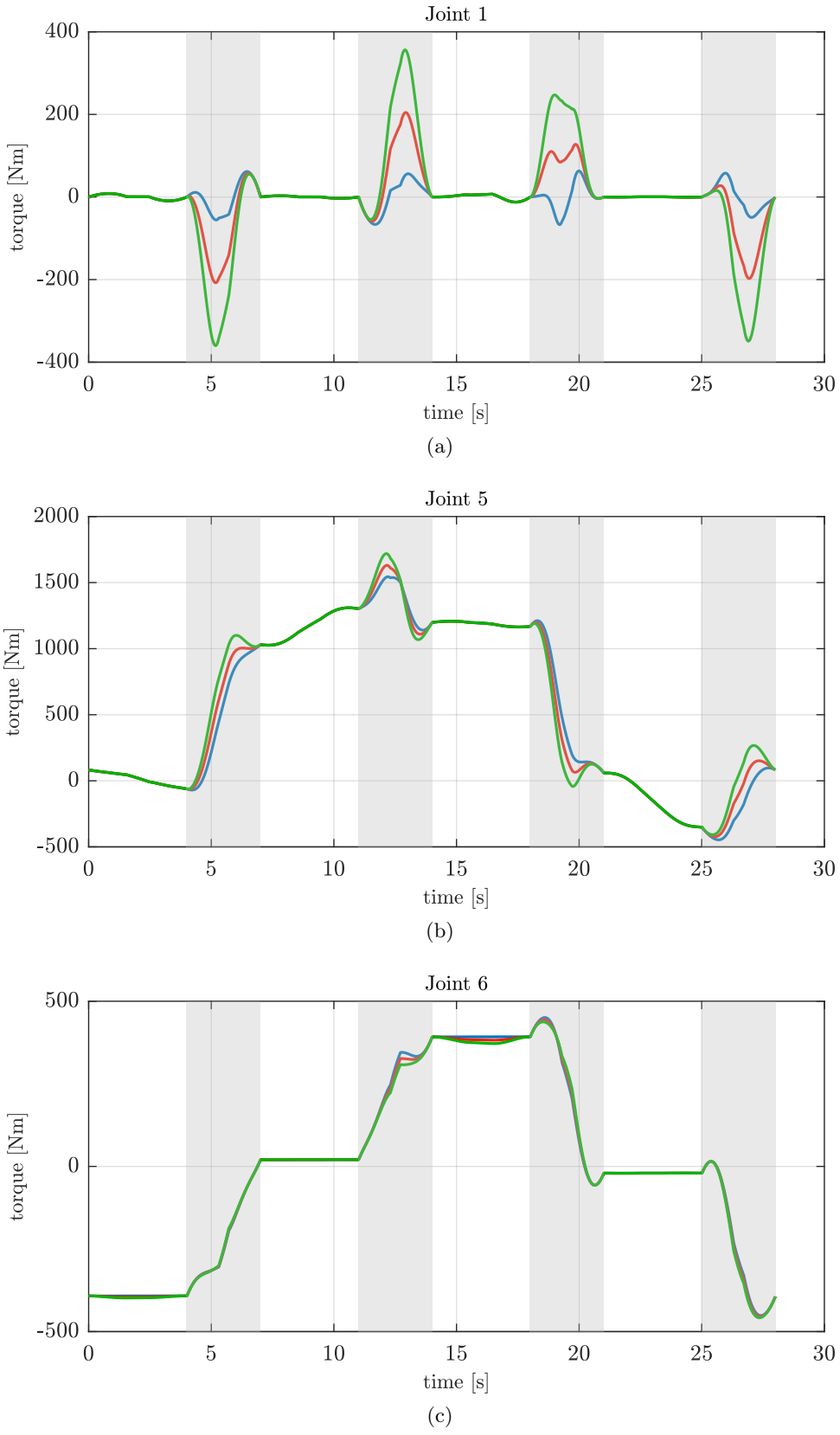

Figure 5.9: Joint torques for different speeds of the grinding disc: **0**, **1500**, **3000** rpm (detail)

first four seconds of the movement. However, here is the difference rather small to be seen on a graph of this size.

The center of mass of the grinding tool is not situated on the last joint axis of the manipulator. Thus, the sixth actuator has to compensate torque exerted by the mass of the grinding tool. Depending on the orientation of the tool, this torque is either almost equal to zero for its vertical orientation or approximately 390 Nm (absolute value) for the horizontal orientation. This can be seen in Figure 5.9c during the time intervals $[7, 11]$ s, $[21, 25]$ s, and $[0, 4]$ s, $[14, 18]$ s when the grinding tool executes only translational movement.

As stated before, the areas highlighted with grey color correspond to the time intervals of grinding tool rotation at the corners of the billet. It is obvious that there is no influence of different grinding speeds on the sixth joint of the robot. Slight difference around time 13 s of the movement is caused by simultaneous movement of other joints. It produces a forced torque on the grinding disc which results into the growth of torque in the sixth joint as discussed above. The axis of joint 5 lays in the plane perpendicular to the axis of forced rotation (axis of the sixth joint). Therefore, there can be observed an influence of gyroscopic effect. Resulting torque depends on the orientation of the grinding tool as well (see Section 4.3), which is why one can not expect explicitly 'increasing' of the torque in individual joints with rise of speed of the grinding tool. Similar action can be seen in the joint 1.

The higher the rate of parallelism between the torque generated by gyroscopic precession and individual joint axes of the manipulator is, the bigger is the influence of the gyroscopic effect. Once these axes are perpendicular to each other, there in no more influence of the gyroscopic effect. This fact can be nicely demonstrated by the torques generated in joint axes 2 and 3. Note that these two axes are always parallel. It can be seen in Figure 5.4 that the joint coordinates of joints 4 and 5 set the axis of joint 6 into a position which is more or less parallel to the axes of joints 2 and 3 all the time. It causes that there is a minimal influence of different speeds of grinding disc. That is why the time behaviour of torques of the second and the third joint are almost identical for different grinding speeds (see Figure 5.7).

5.6 Metal Grinding

This section serves as a brief introduction into the theory of metal grinding. So far the simulation concerned only the forces and moments generated by the weight of links of manipulator and by the gyroscopic effect. Forces needed for machining a metal billet have to be considered in the real application.

A preliminary surfacing in the industrial manufacturing is often executed by grinding which can be described as a scuffing of the product surface by quickly moving grains of an abrasive. Such an abrasive can be shaped as a grinding disc or grinding belt.

The grinding process is influenced by several factors such as a type of ground material and grinding tool, a requirement for the surface roughness or a requirement for the duration of the grinding process.

There are so called cutting forces which are caused by an interaction of the grinding tool and the surface of the ground material. The magnitude of these forces depends on many factors such as a size of a contact area (of the surface and the grinding tool) or required amount of material, which has to be scuffed.

The dynamics of the grinding process is mainly characterized by the resulting cutting force during grinding, which consists of a radial component $\boldsymbol{F}_y$, a tangential component (main cutting force) $\boldsymbol{F}_z$ and an axial $\boldsymbol{F}_x$ component (see Figure 5.10).

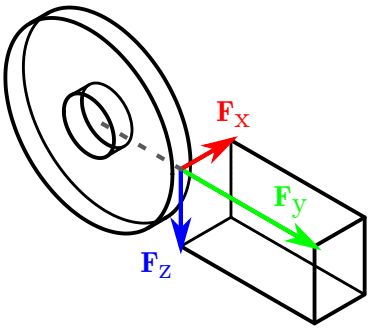

Figure 5.10: Cutting force components

In general, it should hold according [21], that the radial component is always bigger than the tangential one. The ratio of these two forces should be within the interval from $3:1$ ($\boldsymbol{F}_y = 3\boldsymbol{F}_z$) up to $1:1$ ($\boldsymbol{F}_y = \boldsymbol{F}_z$). The axial component is always the smallest one and for further purposes of this thesis will be neglected.

5.7 Grinding with External Forces

A simulation with the same initial condidions as before (see Section 5.3) has been executed in order to investigate an influence of cutting forces on the actuators of the manipulator. The only difference against the first simulation is that in this case cutting forces are considered. As the objective determination of the cutting force magnitude is not possible (no real experiments with any grinding tool have been executed), the radial component of the cutting force has been set to $F_y = 200$ N and the tangential one to $F_z = 100$ N for the experimental purposes. Joint trajectories, velocities and accelerations in this simulation correspond with the values shown in Figures 5.4, 5.5 and 5.6. Resulting torques for individual joints while grinding with external forces are shown in Figure 5.11.

Figure 5.12 shows the difference between joint torques generated by actuators while grinding with an external force and torques caused only by the weight and movement of the manipulator (see Figure 5.7). The curves for different grinding speeds of the disc are identical in the figure.

5.8 Simulation Results

Allowed positions of the robot manipulator in the workspace of grinding station can be considered as one of the results of the simulation. The actuators of the robot are able to compensate torques acting on the system during grinding in allowed positions. Furthermore, the convenience of individual positions of the robot base link with respect to the workpiece can be discussed. It is obvious that some positions of the base link will lead to joint trajectories, which cause less stress in the joints due to their more convenient relative position.

Figure 5.13 shows the ratio of the maximum torque reached during the grinding operation to the maximum allowed torque of respective axis. This ratio is shown for different positions of the robot base link in the grinding station workspace. All positions leading to the overload of the actuators of robot manipulator have been previously removed. As there is not any information about the influence of the counterbalance system of the second link, let's assume, that this device halve the torque which has to be compensated by second actuator (for the context

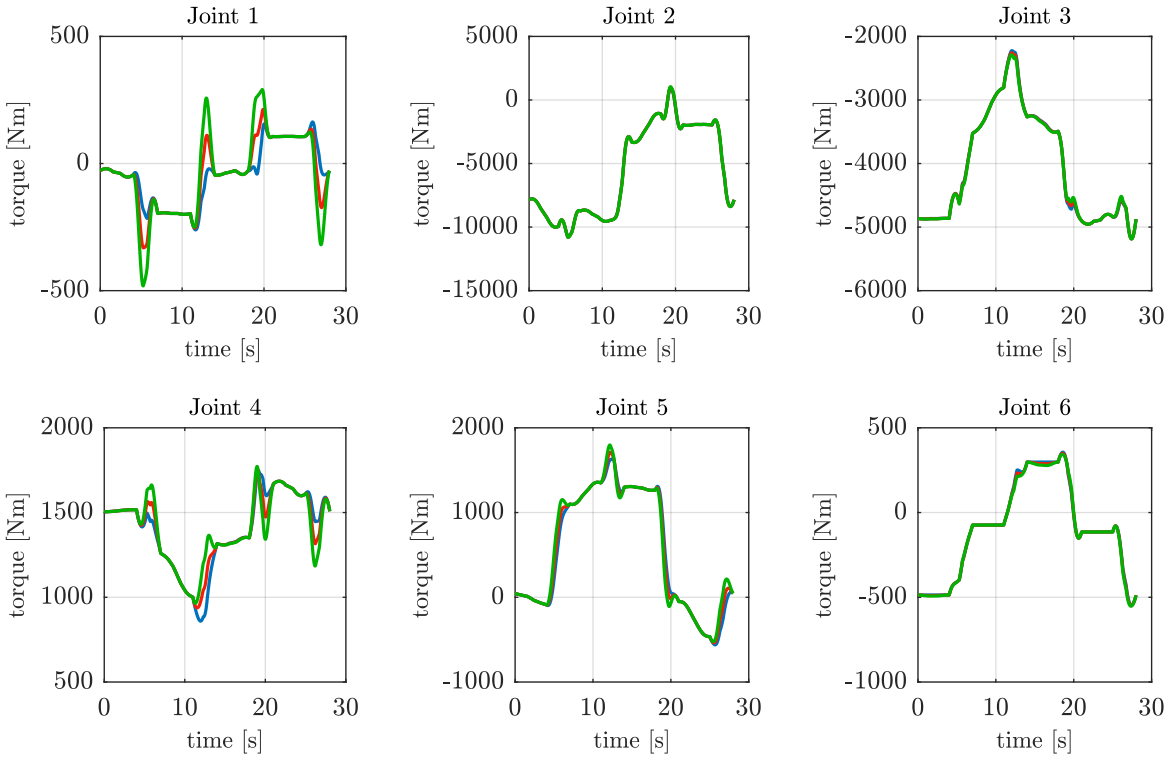

Figure 5.11: Grinding with external forces - joint torques, grinding speeds: **0**, **1500**, **3000** rpm

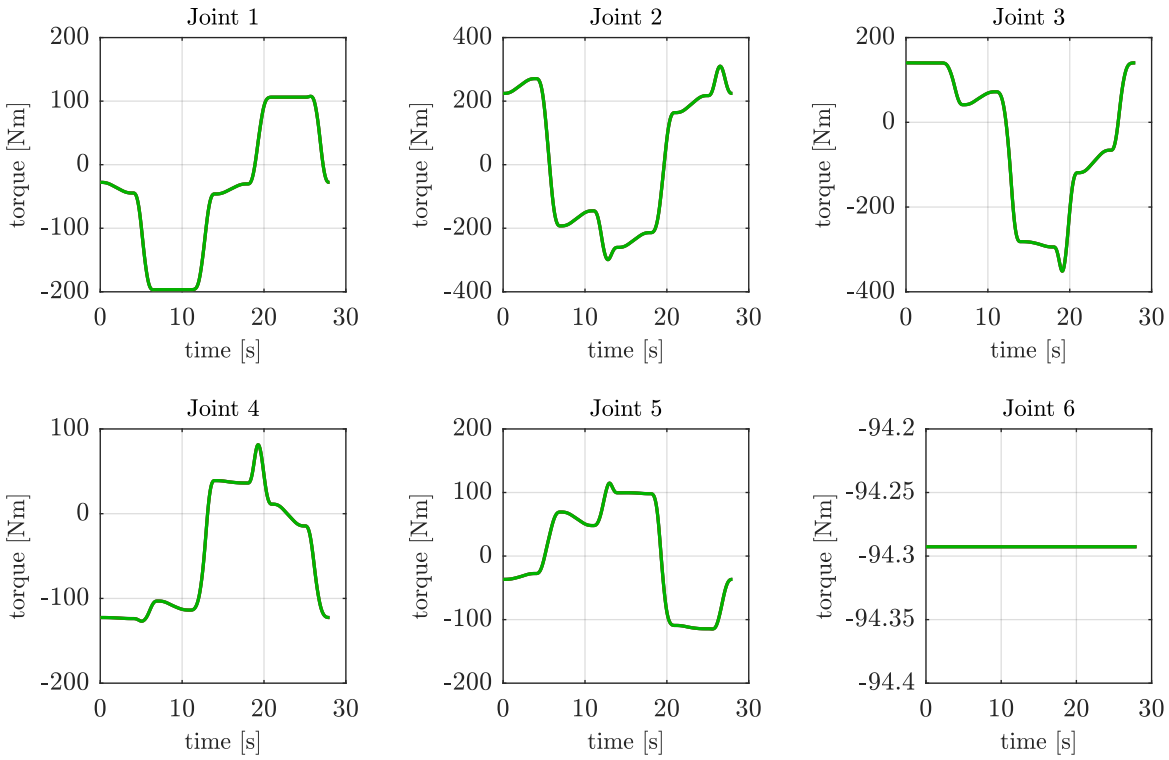

Figure 5.12: Grinding with external forces - difference

see Figure 5.8). Different elevations of the robot base link have been tested (namely from the elevation $z = -1$ [m] to $z = +1$ [m] with a step of length $z = 0.25$ [m]. The elevations higher than $z = 0$ [m] typically lead to higher joint load. On the other hand, the non-positive values of the elevation result into convenient position, where the load of joints is reduced.

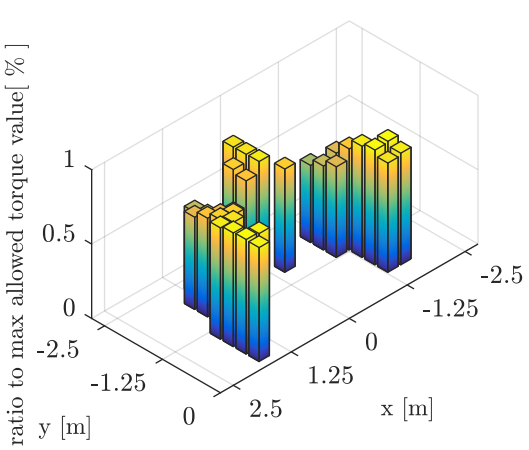

(a) Elevation of robot base position $z = -1$ [m]

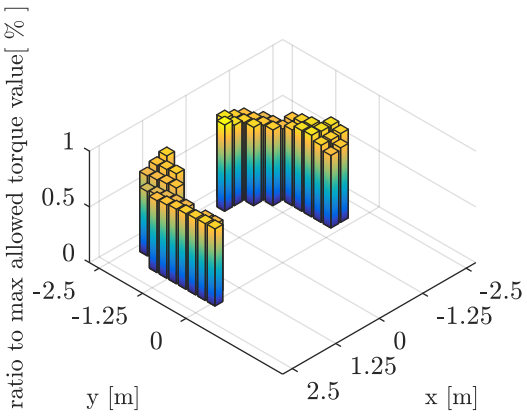

(b) Elevation of robot base position $z = -0.5$ [m]

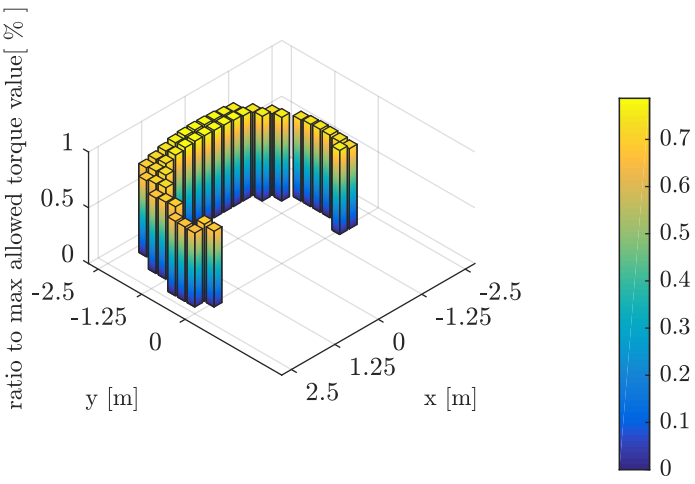

(c) Elevation of robot base position $z = 0$ [m]

Figure 5.13: Position optimization - ratio of maximum reached torque

Figure 5.14 shows the ratio of the maximum of average torque reached during the grinding operation to the maximum allowed torque of respective axis. These values are drawn in positions corresponding to the value of maximum reached torque in Figure 5.13.

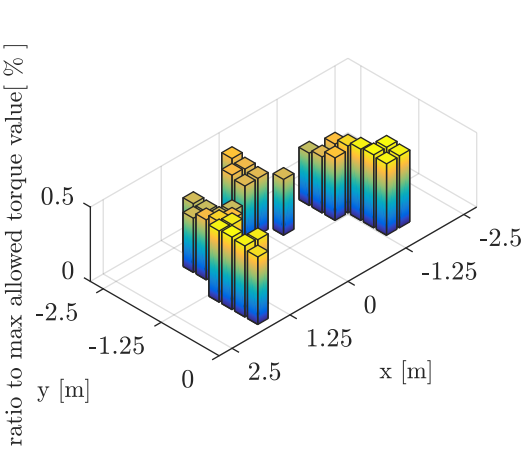

(a) Elevation of robot base position $z = -1$ [m]

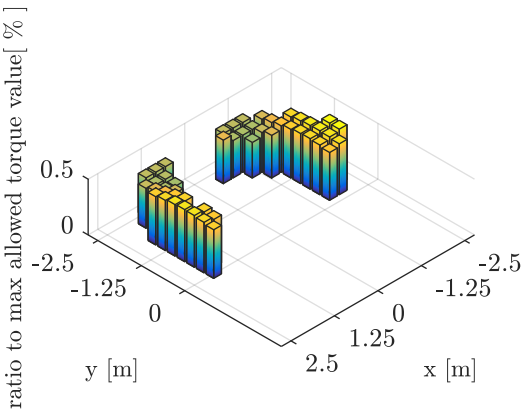

(b) Elevation of robot base position $z = -0.5$ [m]

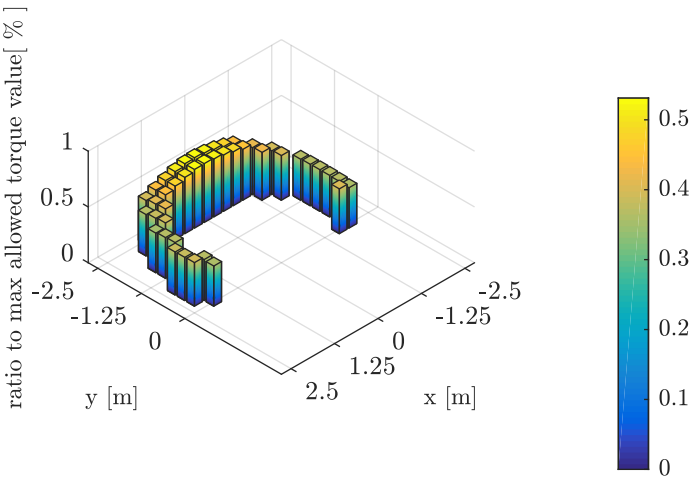

(c) Elevation of robot base position $z = 0$ [m]

Figure 5.14: Position optimization - ratio of average reached torque

6 Experimental Results

This chapter describes an experimental measurement whose main goal is to verify the validity of the approach used in the simulation part, and to confirm the influence of the gyroscopic effect during grinding. There was no requirement for the measurement of exact values corresponding with the results obtained during the simulation. This would not even be possible since there is no appropriate equipment for such an experiment at disposal.

At first, an available system used for the measurement with all its components is described in following sections. Then, a simple grinding tool built for the purpose of experiment is presented and at the end, achieved results are discussed and compared with an expected behaviour of the system.

6.1 System Description

The experiment has been performed using the CloPeMa robotic platform shown in Figure 6.1. The main reason for the use of this manipulator is the fact, that it is equipped with a sensor that is able to measure torques along three axes. This robotic platform (formerly used in the CloPeMa project [22]) is based on robotics components used in the welding industry supplied by Yaskawa Motoman. It consists of two manipulators Motoman MA1400 mounted of the common external axis. The entire system is powered and controlled by a control unit DX100 [22].

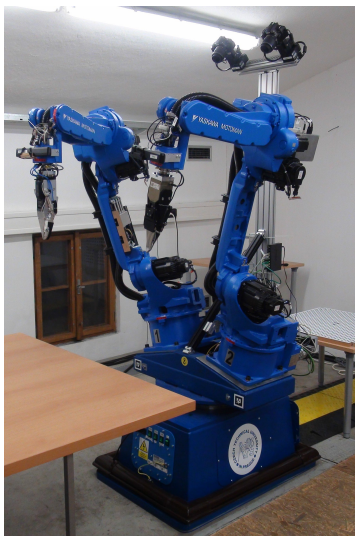

Figure 6.1: Robot manipulator used in the experiment

Both of the robot arms are equipped with the ATI six-axis force/torque sensor (Mini45 FT) mounted on their flanges. This sensor (see Figure 6.2) allows to measure both forces and moments along all three axes of the Cartesian space frame attached to the sensor.

The axes of the sensor are not aligned with the last coordinate frame of the manipulator. As it can be seen in Figure 6.2b, the coordinate frame of the last link of the manipulator (solid lines) and the coordinate frame of the sensor (dashed lines) are rotated. The x-axis is represented by red color and the y-axis is the green one in both frames. The angle between the x-axis of the last link and the axis of symmetry of the sensor is exactly 10 degrees. Rotational offset between the x-axis of the last link (solid) and the x-axis of the sensor (dashed) is 60 degrees. One can easily compute the transformation between those two frames and determine forces and moments represented in the frame of the last link of the manipulator. The same rule holds for any other coordinate frame attached to the manipulator.

Both the positive direction of the z-axis of the last coordinate frame of the robot and the positive direction of the z-axis of the sensor are pointing in the same direction and they are identical. Further details can be found in the datasheet related to the sensor [23].

A couple of calibration measurements have been executed to determine the offset of the sensor of each axis. Each axis of the coordinate frame of the sensor has been pointed towards to the ground (which should generate zero torque in respective axis) and the offset has been read. Measured data have been later modified with respect to found offsets.

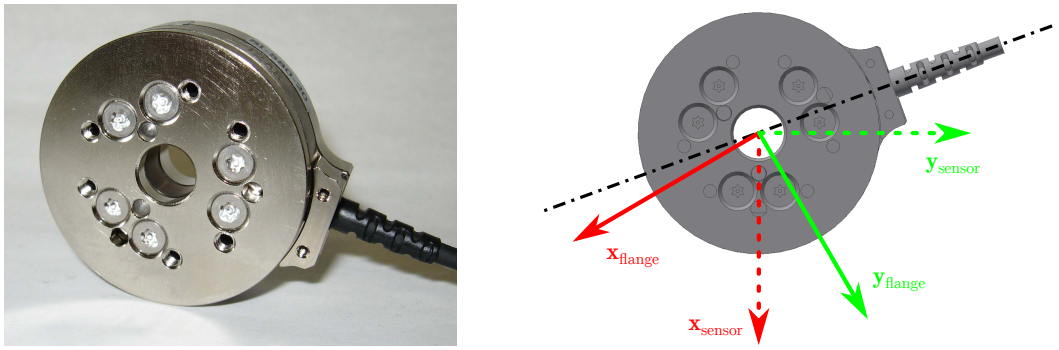

(a) Force/Torque sensor ATI Mini45 [24]

(b) Sensor coordinate system offset

Figure 6.2: Force/Torque sensor

The entire robotic system can be controlled by user's own program written either in C++ or in Python programming language. Robot Operating System (ROS) [25] is used as a middleware that provides connection between the software and the robot controller. ROS also serves as an integration tool for all the different peripheral devices of the robotic platform. An interface using this flexible framework for the control of Motoman MA1400 has been developed during the CloPeMa project. The interface allows the user simultaneously to control the manipulator and to read the data from connected sensors. Both of these features have been used in order to perform the experimental measurements.

6.2 Grinding Tool

A tool, which is able to generate the gyroscopic moment, had to be built for the purposes of the experiment. The allowed payload of the robot MA1400 is only 3 kilograms. Therefore it

was not possible to mount any real grinding machine of the robot to perform an experiment executing actual grinding. This would not even be possible because of the clean environment in the laboratory. Moreover, there is no significant difference between forces acting on the robot during real grinding, and forces which appear during the simulation without the material to be ground as described in Section 5.8. Therefore only the influence of the gyroscopic effect will be verified in the experiment.

A simple *grinding tool* (Figure 6.3) has been built and mounted on the flange of manipulator for the purposes of the experiment. It consists of a three-phase brushless DC motor formerly used in a laser printer. The advantage of this particular motor is the size of its rotor. The rotor is quite heavy and it has a large diameter (in comparison to a common DC motor), which increases the value of the moment of inertia. This property has an essential influence to the gyroscopic moment generated by the rotor.

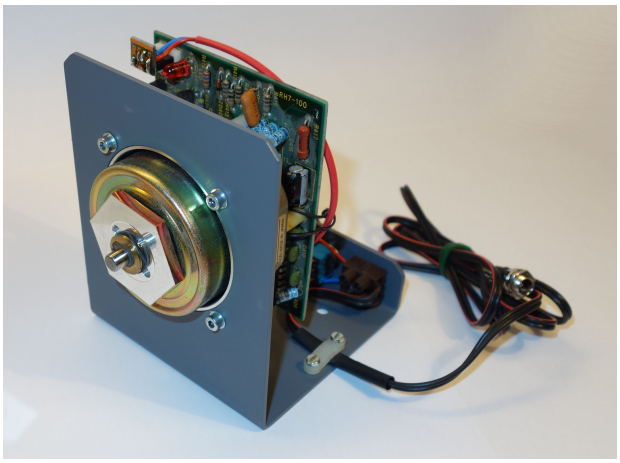

Figure 6.3: Grinding tool for experimental measurement

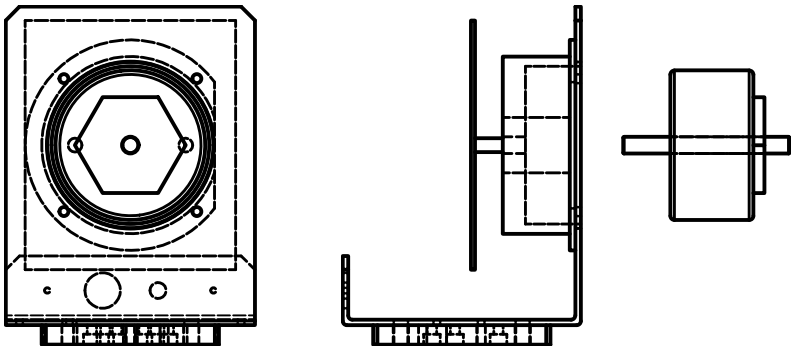

(a) Front view (b) Side view (stator + rotor)

Figure 6.4: Grinding tool for experimental measurement

Autodesk Inventor has been used to design of the grinding tool frame and to estimate of the dynamic parameters of the entire device. The steel frame of the grinding device and the stator of used DC motor are considered to be the sixth link of the manipulator. The rotor represents the grinding disc. Determined dynamic parameters with respect to coordinate frames attached to both bodies (see Figure 6.4) are following:

Metal frame and the stator:

$$m = 0.470 \text{ [kg]} \qquad \boldsymbol{r}_{COG} = [0.00015, -0.03184, 0.01359]^T \text{ [m]}$$
$$\boldsymbol{I} = \begin{bmatrix} 9.79 \cdot 10^{-4} & 0 & 0 \\ 0 & 6.10 \cdot 10^{-4} & 0 \\ 0 & 0 & 9.09 \cdot 10^{-4} \end{bmatrix} \text{ [kg} \cdot \text{m}^2\text{]} \tag{6.1}$$

Rotor:

$$m = 0.205 \text{ [kg]} \qquad \boldsymbol{r}_{COG} = [0, 0, -0.0274]^T \text{ [m]}$$
$$\boldsymbol{I} = \begin{bmatrix} 5.46 \cdot 10^{-5} & 0 & 0 \\ 0 & 5.46 \cdot 10^{-5} & 0 \\ 0 & 0 & 6.89 \cdot 10^{-5} \end{bmatrix} \text{ [kg} \cdot \text{m}^2\text{]} \tag{6.2}$$

6.3 Experiment

Chosen position of the manipulator for the purpose of the experiment is shown in Figure 6.5. Position of the first five axes align the flange of the robot to the horizontal position. The entire manipulator remains motionless and the sixth axis is rotated from position -180 deg about 360 deg during 1.2 second. For time dependence of joint position, velocity and acceleration see Figure 6.6. Several measurements with different joint positions have been performed, however, the position shown in Figure 6.5 produces the most illustrative results. Next reason is that the sixth joint is able to rotate with the highest angular velocity of all joints. Although the rotor is relatively large and heavy (in the measures of similar DC motors), it is still too small to produce high gyroscopic moment. This can be compensated by higher velocity of the axis of forced rotation of the flywheel (grinding tool).

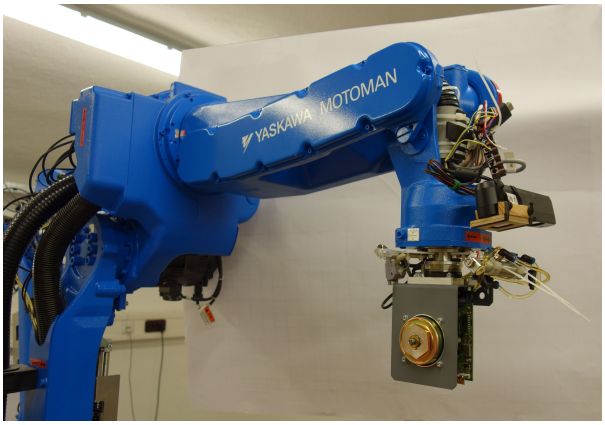

Figure 6.5: Robot position during experiment

Data from the robot controller can be read using the ROS interface during the measurement. Incoming data contains timestamp, corresponding position of individual joints and vector of forces and torques acting on sensor in a format $[F_x, F_y, F_z, M_x, M_y, M_z]^T$. Corresponding velocities and accelerations need to be computed using timestapms and positions of individual joints. As described in Section 6.1, incoming information about forces and moments need to be recomputed into the coordinate frame of required joint to obtain correct values. Incoming data have to be filtered as well because of high rate of noise which can be seen, for example, in Figure 6.7a. This has been done by downsampling and by moving average filtering of the incoming data.

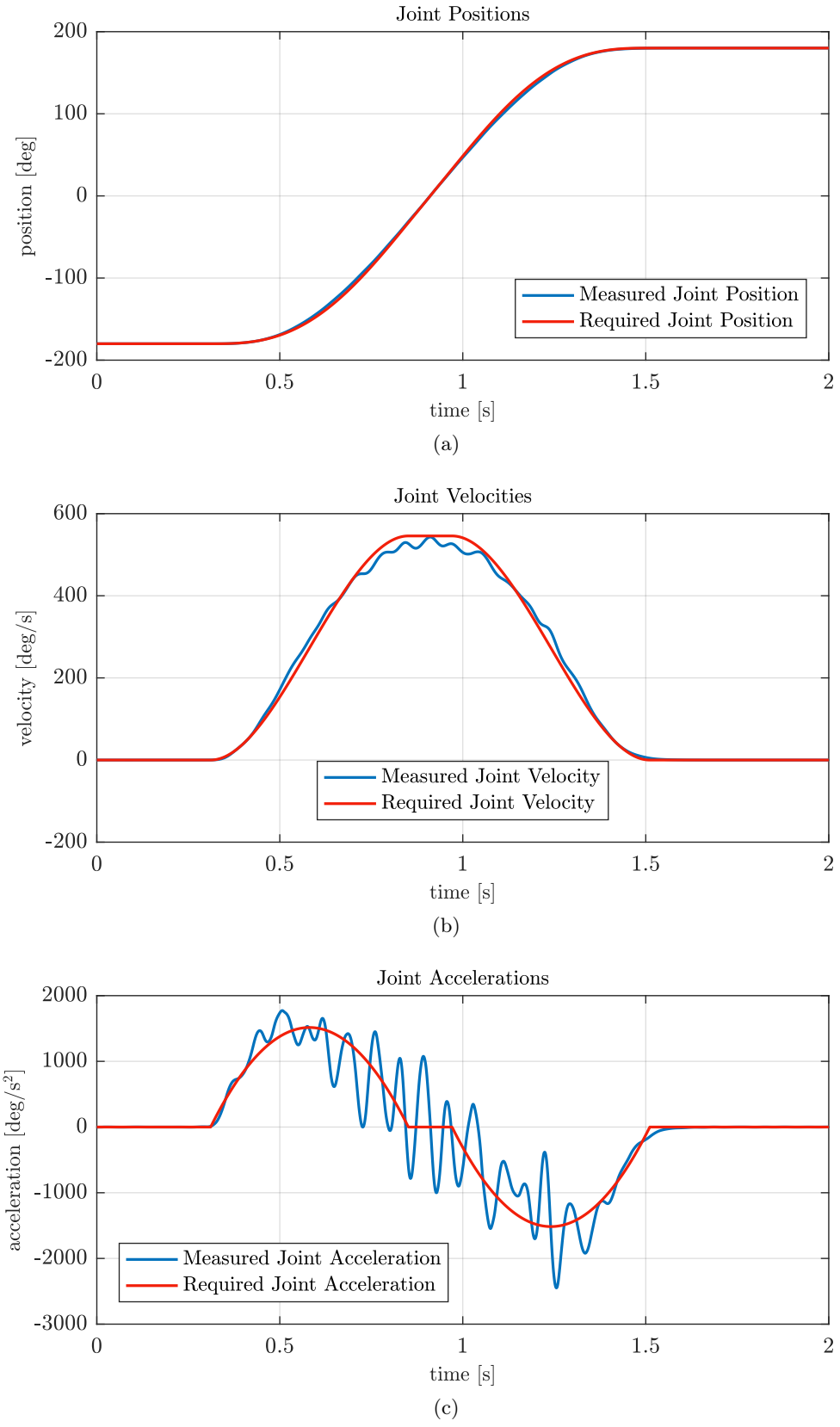

Figure 6.6: Required and measured trajectory of 6-th joint

Required trajectory for the sixth joint shown in Figure 6.6 has been executed simultaneously in the simulator and with the real robot. In both cases the torques have been measured separately for running and stopped disc of the grinding tool (DC motor). Running DC motor rotates with the speed of approximately 4170 rpm. Multiple measurement with the real robot has been performed and resulting data has been filtered and averaged. Torques measured by the sensor and recomputed to the coordinate frame of the last link of manipulator are pictured in Figures 6.7a (grinding tool stopped) and 6.7b (running grinding tool).

The influence of the gyroscopic moment can be easily obtained by subtraction of the torques measured with running grinding tool from the torques measured, while the grinding tool has been stopped. Result of this operation can be seen in Figure 6.7c.

6.4 Results

Figure 6.7a shows measured torques in the coordinate frame of the sixth link during the rotation of the sixth joint with stopped disc of the grinding tool. Torque in the z-axis corresponds with the expected behaviour and depends apparently on the acceleration of the joint. Note, that measured torque has the sign opposite to the torque, which is produced by the actuator. This simply comes from the Newton's third law. Torque measured in the x-axis can be explained by the centrifugal force acting on the entire grinding tool, since its center of mass is not located on the axis of rotation. The torque observed in the y-axis and it's similarity to the torque of the z-axis would require further measurements and research. Expected value of torque for this axis is zero (as the x-coordinate of the center of mass is located almost on the axis of rotation) or a peak with much smaller magnitude, which can be observed in the x-axis.

Figure 6.7b shows nice demonstration of the influence of gyroscopic moment. Rotating disc of the grinding tool produces torque which fully suppresses the influence of the centrifugal force. Torques in the y and z-axis do not significantly change due to the influence of gyroscopic moment.

Figure 6.7c represents the pure influence of the gyroscopic effect. As it can be seen in this figure, the torque generated by this effect points in the positive direction of the x-axis of the last link the entire time of movement. Its magnitude depends strongly on the velocity of forced rotation (rotation of the sixth joint), on the inertia property and on the angular velocity of the grinding disc (which cannot be observed due to fixed speed of the DC motor). This figure proves among other things the fact, that torque generated in the sixth joint does not depend on the speed of rotating disc at all.

Resulting torques recomputed into individual joint frames are shown in Figure 6.8. As it is obvious from the figures, measured torques are really small. Torques obtained from the simulation for the fourth and the fifth joint almost precisely correspond with the torques measured by the sensor (except of the sign of the values, which has been set to negative for measured torques as discussed above). The torque measured in the sixth axis differs slightly from simulation output. The difference in magnitude could be explained by wrong offset gained during the calibration measurement. Further measurements and research would be necessary to explain the difference in the curve shape of measured torque. However, as stated before, the experimental measurement had to prove that the results of simulation generally correspond with the real world, not to measure exact values.

Even in a case it is not necessary to compensate the torque caused by gyroscopic moment (because of its orientation) directly by an actuator, this force has an influence on the body and especially on the joint bearings.

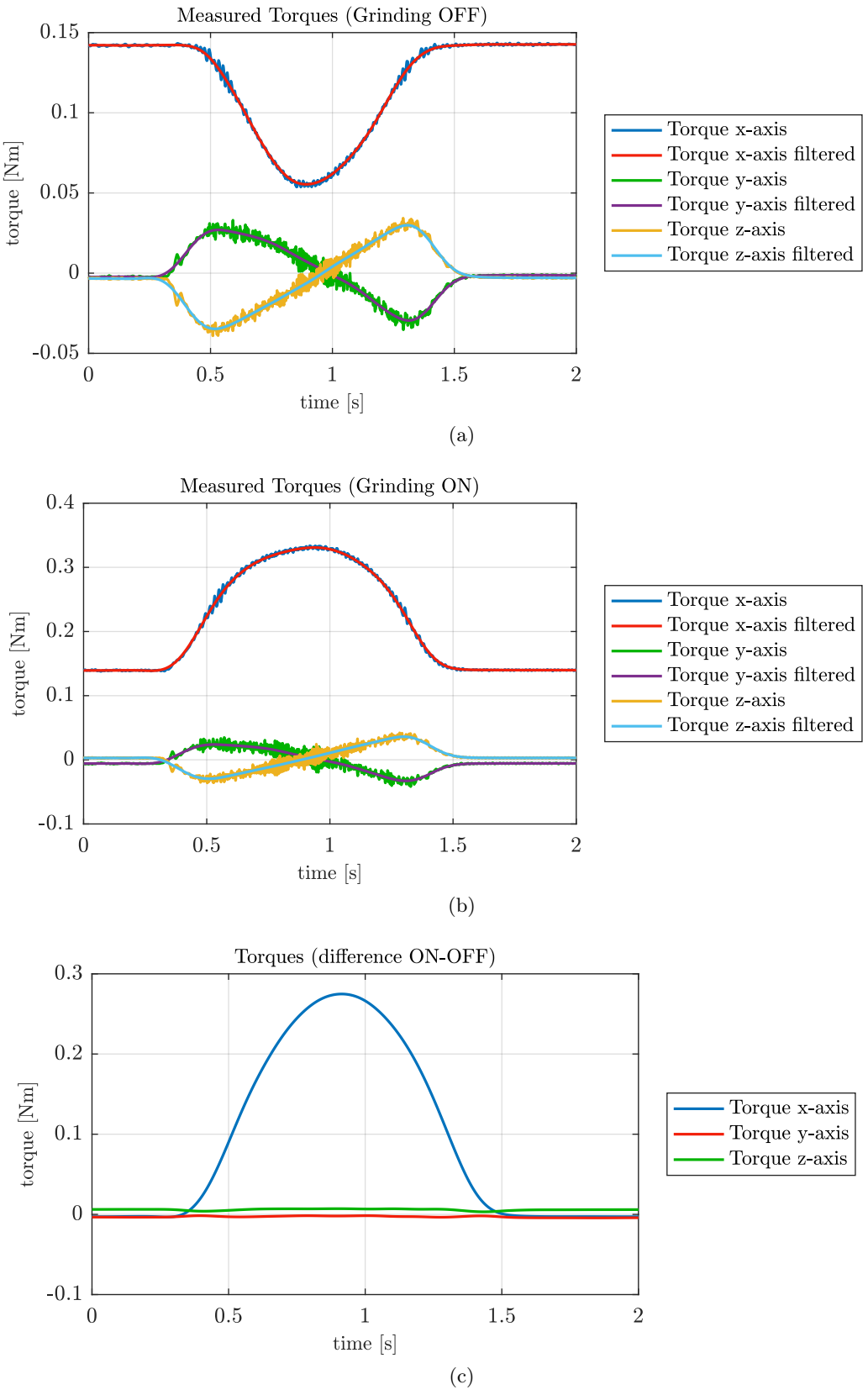

Figure 6.7: Measured torques (converted into the flange coordinate frame)

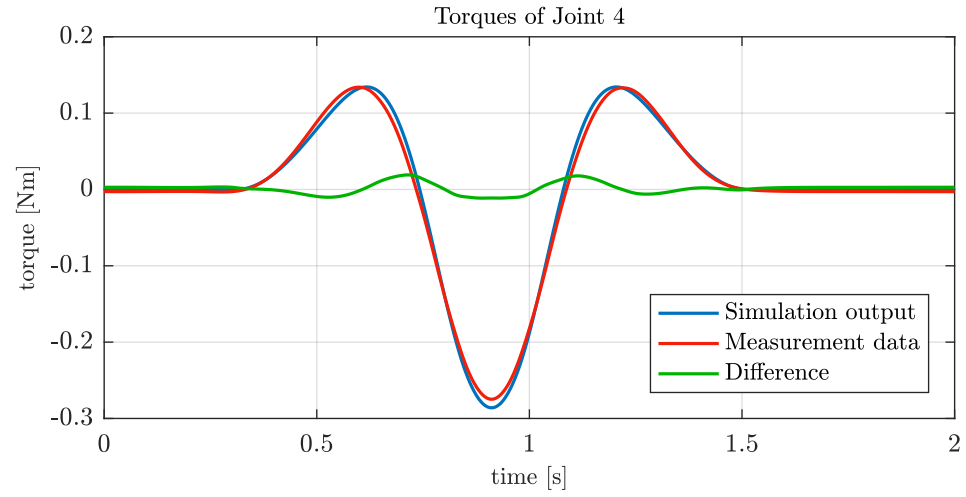

(a)

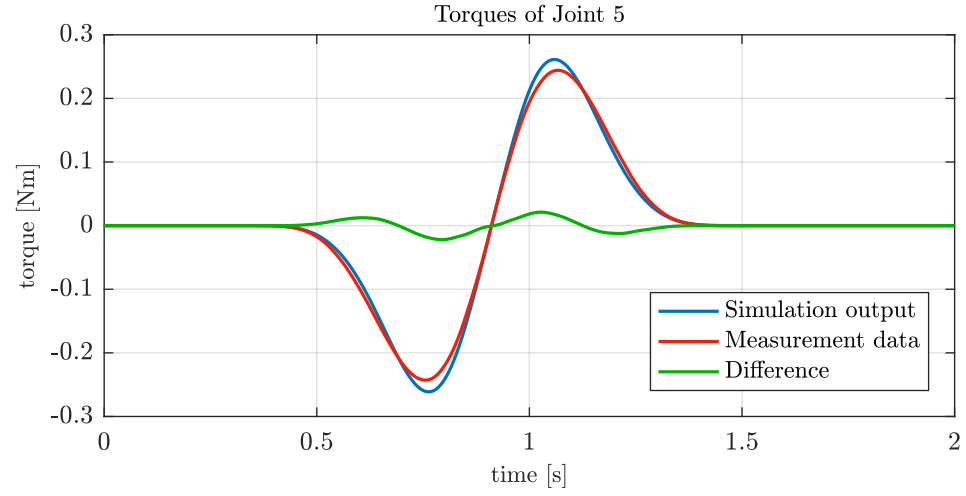

(b)

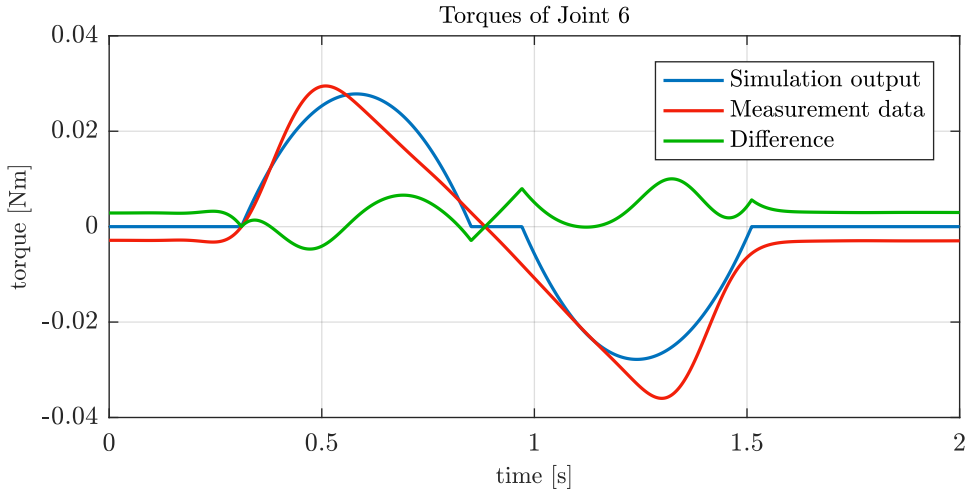

(c)

Figure 6.8: Comparison of simulated and measured torques

7 Conclusion

This thesis deals with the forces acting on the industrial manipulator during grinding. The influence of heavy rotating masses at the position of the end-effector of the robot was investigated using the method for dynamic modelling of rigid-bodies. Further, the suitability of the proposed manipulator KUKA KR 500 R2830 MT for the grinding operation was discussed and tested with computer simulations. At the end, the implemented solution to the dynamic modelling of robot manipulators was verified using the different manipulator, namely Motoman MA1400.

7.1 Conclusion

The process of metal manufacturing in the hot rolling mill and the need for deploying the six-axis robot manipulator for the task of machining of the workpieces is described at the beginning of this thesis. The proposed solution with the grinding tool mounted on the flange of the robot requires an analysis of the torques, which have to be compensated by the actuators of the manipulator. Heavy rotating masses at the position of the end-effector generate gyroscopic moment, which has to be additionally compensated by the actuators. The capability of the manipulator KUKA KR 500 R2830 MT to perform the grinding operation was investigated.

The kinematic model including the solver for both the direct and for the inverse kinematic task of the KUKA KR 500 manipulator has been built in order to plan joint trajectories for required movements of the grinding tool during the machining process. The dynamic simulations performed with the manipulator require both the kinematic model and the dynamic parameters. Since these parameters are not included in the product datasheets, and the manufacturer does not provide this information, necessary parameters have been estimated using 3D CAD model and the Autodesk Inventor software.

The dynamic model of the manipulator has been created using the recursive Newton-Euler approach. This method appeared to be suitable especially for the open kinematic chains and its use is straightforward even for six-axis robot manipulators. The general influence of the gyroscopic effect on the system is described and demonstrated in the simple example.

Simulations for different scenarios were performed. The grinding of the billet with a quadratic cross-section appeared to be more complex task, thus it has been chosen as a demonstration example in this thesis. The results of the simulation prove, that suggested manipulator should be capable to perform the grinding operation. However, simulation results still suffer from missing accurate information. Dynamic parameters that have been found using Autodesk Inventor does not fully correspond to the reality and there is still the missing information about the counterbalance of second link of the manipulator. The simple optimization procedure was performed in order to find more convenient positions relative to ground billet.

Implemented solution of the modelling of dynamics was verified during the experimental measurement with the real robot Motoman MA1400 and the Force/Torque sensor ATI Mini45. The results of measurement approximately correspond with the results of simulation, which proves the validity of implemented solution.

7.2 Recommendation for Future Work

Dynamic parameters have the significant influence on the results of simulations. These parameters were estimated using the 3D CAD model of respective manipulator for the purposes of this thesis. This approach appeared to be the most accurate available method for the estimate. However, it is still not possible to obtain certain information even with the detailed CAD model. For example, the influence of the counterbalance system cannot be determined this way. Thus, it would be useful to perform the simulations again and to see the difference with accurate values obtained by, for example, dynamic identification of the real robot.

The designed model of the grinding tool used in the simulations is completely based on current solution of the grinding station. This concept is definitely not optimal for mounting on an industrial manipulator. The measurements necessary for an optimization of new grinding machine would be reasonable attitude in order to prevent using of a similar overdesigned device. Optimized grinding machine could result in some kind of more light-weight solution, which would cause a requirement for a manipulator with lower payload (and possibly lower cost).

The Recursive Newton-Euler Algorithm enables to compute both the required torque to be generated by an actuator and the forces and torques acting within the joint, for example, on the bearings. This additional information could be further used for the estimate of a wear of the inner components of the manipulator. Such information could be possibly used for planning of the regular maintenance or to avoid to mechanical malfunction.

References

[1] ifm electronic, s.r.o. Image, procedure and components description: Hot Rolling Mill. http://www.ifm.com/ifmcz/web/apps-by-industry/cat_040_020.html, [Online; accessed May 12, 2017].

[2] Ing. Petr Farkavec. [digital image], 2017.

[3] KUKA AG. *KUKA Roboter für schwere Traglasten*, 2017. PB0005/D/3/0514.

[4] KUKA AG. *Pub Spez KR 500 MT FORTEC (PDF) de*, 03 2016. Spez KR 500 MT FORTEC V3.

[5] Yonghua Chen and Fenghua Dong. Robot machining: recent development and future research issues. *The International Journal of Advanced Manufacturing Technology*, 66(9):1489–1497, 2013.

[6] Zengxi Pan and Hui Zhang. Robotic machining from programming to process control. *Robot Manipulators New Achievements*, 2010. ISBN: 978-953-307-090-2.

[7] Zengxi Pan, Hui Zhang, Zhenqi Zhu, and Jianjun Wang. Chatter analysis of robotic machining process. *Journal of Materials Processing Technology*, 173:301–309, 2006.

[8] Marthin Krantz and Rikard Andersson. Robotized polishing and deburring with force feedback control. Master's thesis, University West, Department of Engineering Science, Trollhättan, Sweden, 2010.

[9] R. S. Hartenberg and J. Denavit. A kinematic notation for lower pair mechanisms based on matrices. *Journal of Applied Mechanics*, 77:215–221, 1955.

[10] Ing. Vladimír Smutný, Ph.D. Forward and Inverse Kinematics of Serial Manipulators, CTU Lecture. http://cmp.felk.cvut.cz/cmp/courses/ROB/roblec/, [Online; accessed May 06, 2017].

[11] Ing. Vladimír Smutný, Ph.D. Inverse Kinematics of 6–DOF Serial Manipulator, CTU Lecture. http://cmp.felk.cvut.cz/cmp/courses/ROB/roblec/, [Online; accessed May 06, 2017].

[12] Claudio Gaz, Fabrizio Flacco, and Alessandro De Luca. Identifying the dynamic model used by the kuka lwr: A reverse engineering approach. In *2014 IEEE International Conference on Robotics & Automation (ICRA)*, 2014.

[13] N.L.D. Marck. Semi-parametric identification of manipulator dynamics in a timevarying environment. Master's thesis, Delft University of Technology, 2017.

[14] Roy Featherstone. *Rigid Body Dynamics Algorithms*. Springer, 2008.

[15] Mark W. Spong, Seth Hutchinson, and M. Vidyasagar. *Robot Modeling and Control*. Wiley, 2006.

[16] Herman Høifødt. Dynamic modeling and simulation of robot manipulators. Master's thesis, Norwegian University of Science and Technology, 2011.

[17] R. N. Jazar. *Theory of Applied Robotics: Kinematics, Dynamics, and Control*. Springer, 2010.

[18] Walter Lewin. Rolling Motion, Gyroscopes | 8.01 Classical Mechanics, MIT Lecture, 1999. https://youtu.be/N92FYHHT1qM, [Online; accessed May 06, 2017].

[19] Vsevolod Aleksandrovič Pavlov. *Giroskopičeskij effekt: jego projavlenija i ispolźovanije*. Leningrad: Sudostrojenije, 1972.

[20] Eugenio Yime-Rodríguez, César Augusto Peña-Cortés, and William Mauricio Rojas-Contreras. The dynamic model of a four control moment gyroscope system. *DYNA*, 81(185):41–47, 2014.

[21] J. N. Maslov. *Teorie broušení kovů*. SNTL - Nakladatelství technické literatury, n. p., 1979. L13-B2-V-31f/22649.

[22] CloPeMa. http://www.clopema.eu/, [Online; accessed May 16, 2017].

[23] ATI Industrial Automation. *Mini45-E Transducer with Strain Relieved Cable*, 2007. 9230-05-1315.

[24] ATI Industrial Automation. Image: Force/Torque Sensor Mini45-E. http://www.ati-ia.com/products/ft/ft_models.aspx?id=Mini45, [Online; accessed May 12, 2017].

[25] Robot Operating System (ROS). http://www.ros.org/, [Online; accessed May 16, 2017].

CD Content

Directory name	Description
documents	related materials, datasheets, drawings
images	images used in thesis
sources	source codes
thesis	diploma thesis